HHS Public Access

Author manuscript

Appl Sci (Basel). Author manuscript; available in PMC 2024 January 18.

Published in final edited form as:

Appl Sci (Basel). 2023 April 02; 13(8): . doi:10.3390/app13085021.

Transformative Technology for FLASH Radiation Therapy

Reinhard Schulte[1,*], **Carol Johnstone**[2], **Salime Boucher**[3], **Eric Esarey**[4], **Cameron G. R. Geddes**[4], **Maksim Kravchenko**[3], **Sergey Kutsaev**[3], **Billy W. Loo Jr.**[5], **François Méot**[6], **Brahim Mustapha**[7], **Kei Nakamura**[4], **Emilio A. Nanni**[8], **Lieselotte Obst-Huebl**[4], **Stephen E. Sampayan**[9,10], **Carl B. Schroeder**[4], **Ke Sheng**[11], **Antoine M. Snijders**[4], **Emma Snively**[8], **Sami G. Tantawi**[8], **Jeroen Van Tilborg**[4]

[1]Division of Biomedical Engineering Sciences, Loma Linda University, Loma Linda, CA 92350, USA

[2]Fermi National Accelerator Laboratory, Batavia, IL 60510, USA

[3]RadiaBeam Technologies, LLC, Santa Monica, CA 90404, USA;

[4]Lawrence Berkeley National Laboratory, Berkeley, CA 94720, USA

[5]Department of Radiation Oncology, Stanford University School of Medicine, Stanford, CA 94305, USA

[6]Brookhaven National Laboratory, Upton, NY 11973, USA

[7]Argonne National Laboratory, Lemont, IL 60439, USA

[8]SLAC National Accelerator Laboratory, Menlo Park, CA 94025, USA

[9]Lawrence Livermore National Laboratory, Livermore, CA 94551, USA

[10]Opcondys, Inc., Manteca, CA 95336, USA

[11]Department of Radiation Oncology, University of California, San Francisco, CA 94115, USA

Abstract

The general concept of radiation therapy used in conventional cancer treatment is to increase the therapeutic index by creating a physical dose differential between tumors and normal tissues through precision dose targeting, image guidance, and radiation beams that deliver a radiation dose with high conformality, e.g., protons and ions. However, the treatment and cure are still limited by normal tissue radiation toxicity, with the corresponding side effects. A fundamentally

*Correspondence: rschulte@llu.edu.

Author Contributions: Conceptualization, R.S., C.J., S.B., S.K., B.W.L.J., F.M., B.M., K.N., L.O.-H., S.E.S., K.S. and A.M.S.; software, C.J.; formal analysis, M.K., L.O.-H. and A.M.S.; investigation, K.N., E.A.N., L.O.-H., S.E.S., A.M.S., E.S. and S.G.T.; resources, E.E., C.G.R.G., C.B.S. and J.V.T.; data curation, M.K., K.N., L.O.-H. and A.M.S.; writing—original draft preparation, R.S., C.J., S.B., S.K., B.W.L.J., F.M., B.M., L.O.-H., S.E.S. and E.S.; writing—review and editing, R.S., C.J., S.B., M.K., S.K., B.W.L.J., F.M., B.M., E.A.N., S.E.S., C.B.S., K.S., A.M.S., E.S., S.G.T. and J.V.T.; visualization, C.J.; supervision, E.E., C.G.R.G., C.B.S., J.V.T., K.S., E.E. and C.G.R.G.; project administration, E.E. and C.G.R.G.; funding acquisition, F.M. All authors have read and agreed to the published version of the manuscript.

Institutional Review Board Statement: Not applicable.

Informed Consent Statement: Not applicable.

different paradigm for increasing the therapeutic index of radiation therapy has emerged recently, supported by preclinical research, and based on the FLASH radiation effect. FLASH radiation therapy (FLASH-RT) is an ultra-high-dose-rate delivery of a therapeutic radiation dose within a fraction of a second. Experimental studies have shown that normal tissues seem to be universally spared at these high dose rates, whereas tumors are not. While dose delivery conditions to achieve a FLASH effect are not yet fully characterized, it is currently estimated that doses delivered in less than 200 ms produce normal-tissue-sparing effects, yet effectively kill tumor cells. Despite a great opportunity, there are many technical challenges for the accelerator community to create the required dose rates with novel compact accelerators to ensure the safe delivery of FLASH radiation beams.

Featured Application:

We report on new accelerator technology that has applications in FLASH radiation therapy. FLASH radiation therapy may have profound implications in cancer therapy because it may significantly spare normal tissues and solve the problem of tumors in motion due to the short time interval (sub-second) during which it is delivered.

Keywords

particle accelerators; FLASH effect; radiation therapy

1. Introduction

Radiation therapy is a dynamic research field driven by new technology developments. An exciting recent discovery is the sparing of normal (non-tumor) tissues when irradiated with ultra-high dose rates, but tumors are not spared when irradiated with the same radiation field, as first reported by Favaudon and colleagues in 2014 [1]. This phenomenon, which is now called the FLASH effect, opens up a potential new modality in radiation therapy (RT). Tissue sparing means that much higher radiation doses than conventional ones are tolerated, increasing the potential for a cure with an accompanying reduction in side effects.

Many preclinical and first clinical results indicate a dramatic reduction of the toxicity response at FLASH-RT dose rates compared to conventional dose rates. The first human patient was treated with FLASH RT in 2019 at CHUV, a 75-year-old man with progressive cutaneous T-cell lymphoma presenting with multiple skin lesions. Between 2008 and 2018, the patient was treated with conventionally fractionated RT 110 times for painful or ulcerated lesions. This led to local tumor control at those sites but was often associated with poor skin tolerance. FLASH RT was delivered to a previously untreated tumor site at a dose of 15 Gy with 5.4 MeV electrons in 90 ms [2]. Of note, the same dose of 15 Gy was delivered on the same day in 2.87 min as conventional electron therapy to another untreated lesion of similar size, allowing a comparison of the two modalities in the same patient. The skin reaction was minimal (grade 1) in both treated lesions, and the surrounding skin appeared normal 85 days after either FLASH or conventional radiotherapy. These first human data demonstrated that the dose range, if any, where noticeable improvement in human skin tolerance with FLASH RT occurs, is currently unknown [3]. At CHUV,

a dose-finding study has been initiated with a clinical trial (IMPulse, NCT04986696) in refractory metastatic melanoma [4].

Most FLASH experiments and preclinical studies have been performed with electrons and, more recently, with cyclotron-generated protons. However, conventional radiotherapeutic electron beams (4–25 MeV) cannot penetrate enough to treat deep-seated tumors and are thus not likely to be widely used clinically for FLASH-RT. The distal dose fall-off of electrons in tissue is quite shallow as electrons are scattered and have considerable energy straggling, especially at low energies. Protons are currently the most commonly used heavy-charged particle in RT with a Bragg peak dose and finite range advantage. They are also beginning to be used for the first treatment-planning studies for clinical trials with FLASH-RT [5,6] as well as clinical trials. For example, FAST-01 (NCT04592887) is a feasibility study of FLASH RT for the treatment of symptomatic bone metastases that completed recruitment and has been reported [7,8], and FAST-02 (NCT05524064) is a follow-up clinical trial of FLASH RT for the treatment of symptomatic bone metastases in the thorax, currently recruiting. Heavy ions, such as carbon and helium, are not widely used despite a potentially much greater therapeutic effect due to the high linear energy transfer (LET). The high associated costs of ion accelerator and gantry technologies have prevented their widespread use. However, several carbon ion facilities are operational in Europe and Asia, particularly Japan.

Considerable research and development (R&D) in this area is essential for optimizing and clinically realizing the curative potential of FLASH-RT with different radiation modalities. Currently, electron FLASH studies are performed using dedicated 4–6 MeV electron research accelerators that have been optimized for delivering FLASH radiation (Kinetron and Oriatron) or modified medical linacs, originally designed for treatment with electrons or X-rays (see [4] and references therein). These studies provide the strongest, most consistent preclinical evidence for the FLASH effect. Experimental high-dose-rate photon beams were used in the 1960s to demonstrate the in vitro sparing of Chinese hamster ovary (CHO) cells by single X-ray pulses of a nanosecond length [9]. The observed sparing effect above a certain dose rate (order of 10^9 Gy/s) was interpreted as the effect of local oxygen depletion, which took place too fast for oxygen diffusion to maintain an adequate oxygenation level. High-dose-rate photon beams can also be formed using light-source synchrotrons. The FLASH effect has also been observed with protons using shoot-through beams from clinical continuous-wave (CW) or isochronous cyclotrons (iso-cyclotrons) [10]. In shoot-through beams, the beam is not energy-degraded, so the proton energy ranges from 230–250 MeV, i.e., the highest available proton energy with these cyclotrons. Synchrotrons, even the rapid-cycling 15 Hz ion synchrotron being developed at Brookhaven National Laboratory (BNL), cannot produce the intense ion beams required for a clinical application of FLASH-RT, and only a very small volume can be irradiated at the cycle time of the synchrotron.

The purpose of this article is to review the technological underpinning of FLASH-RT with an emphasis on new developments in accelerator technology suitable for producing FLASH conditions. Readers interested in the radiobiological basis of the FLASH effect are referred to review articles on this topic, e.g., ref. [11].

2. Beam Conditions for the FLASH Effect

Preclinical electron studies and other studies with non-electron radiation modalities and in different laboratories support the general impression that FLASH effects are observed for mean dose rates above 40 Gy/s, but for a full effect, dose rates equal to or higher than 100 Gy/s may be required [10,12–15]. The FLASH effect has been observed for a wide range of instantaneous dose rates (IDR), both for single and multiple pulses and CW delivery, as seen in Figure 1.

The single proton outlier in Figure 1 could reflect a difference between the beam structure of the quasi-continuous wave (quasi-CW) proton therapy beam and the 100–300 Hz pulsed electron beam, which has an RF bunch microstructure. The RF GHz bunch microstructure of the electron beam is approximately two orders of magnitude shorter than the MHz RF bunch structure of the proton beam. However, the explanation that the absence of FLASH protection is due to the several-orders-of-magnitude-lower dose rate in the CW proton bunches compared to electron pulses (10^3 vs. 10^6 Gy/s) is not supported by later data from Oncoray in Dresden [16] as well as the growing body of literature evidence showing that isochronous proton beams do produce a FLASH effect in various biological systems despite the lower IDR of the proton bunches compared to the IDR of electron pulses used for FLASH RT.

2.1. FLASH with Electron Beams

Highlights of the observed FLASH effects from the <20 MeV electron beams produced by clinical linacs using pulse repetition rates up to 300 Hz are listed below with references. Beam properties from a compilation of studies observing FLASH electron beam conditions are summarized in Table 1.

- Study of pulmonary fibrosis from irradiation of the lung [1]: Severe to moderate fibrosis for the conventional average dose rate of 0.03 Gy/s, with a 17 Gy total dose. For an average dose rate of 40–60 Gy/s, the equivalent fibrosis occurred at a 30 Gy total dose.
- Study of neurocognitive impairment in mice from brain irradiation [14]: Severe neurocognitive degeneration at an average dose rate of 0.1 Gy/s, with a 10 Gy total dose. Reduced impairment starts at 30 Gy/s with no neurocognitive decline at 100 Gy/s, with an average dose rate for 10 Gy.
- Skin irradiation (mini-pig) [13]: Fibrosis and necrotic lesions were observed at an average dose rate of 0.08 Gy/s (22–37 Gy total dose), with only mild depigmentation at an average dose rate of 300 Gy/s (22–37 Gy total dose).

Additionally, there are proposals for very-high-energy electron beams (VHEE) for a more penetrating clinical electron beam. Tumor depths of 30 cm require 200–250 MeV electrons. Treatment models have predicted that delivering 10 Gy/s requires 10^{11} e/s for a 200 MeV, σ = 1.5 mm Gaussian beam (D. Bartosik, personal communication, May 2021). Although not discussed in depth here, there are existing electron accelerator facilities that could be used for FLASH studies. The 5 Hz FAST SRF Linac at Fermilab produces 50 and 300 MeV beams capable of delivering up to 1000 Gy/pulse and a 10^6 Gy/s instantaneous rate based

on the above simulation. Clinical scanning capability requires a faster duty cycle of ~100 Hz or higher. The CBETA CW recirculating energy recovery linac at Cornell University produces a 150 MeV beam and can scan 10^6 Gy/s at 200 cm/ms (beyond current transverse scanning capability). The size of the ring can be dramatically reduced by replacing the weak permanent magnets in the arcs and a miniaturized version is under conceptual design.

2.2. FLASH with Photon Beams

Megavoltage (MV) photon dose rates produced using clinical electron linacs are too low, and no FLASH effects have been observed. The first photon FLASH dose rates were produced using dedicated pulsed kVp X-ray tubes built in the 1950s and 1960s at the Atomic Energy Research Establishment (AERE). An in vitro study published in 1969 using high-dose-rate X-rays delivered with a single sinusoidal nanosecond pulse of ~10 ns or 50 ns lengths to mammalian cells showed cell survival sparing effects compared to 60Co gamma rays of a conventional dose rate [9]. In recent years, Monte Carlo simulations and experimental validation with scintillators provided evidence that unfiltered 160 kVp X-ray tubes can provide FLASH dose rates exceeding 40 Gy/s or even 100 Gy/s but only over a shallow-water-equivalent penetration depth of <2 mm [17,18]. A pair of opposing X-ray sources can achieve a better dose uniformity at the depth. Based on this concept, a system for small-animal FLASH research has recently been developed by a group of investigators at Johns Hopkins University using commercially available high-capacity 150 kVp X-ray sources with rotating anode technology and validated with GEANT4 Monte-Carlo simulations [19]. A FLASH dose rate can also be generated using a high-intensity superconducting radio-frequency (SRF) electron linac with a tungsten target producing intense higher-energy photon beams (6–8 MeV) at the Chengdu THz Free Electron Laser facility. A significant FLASH effect in tumor-bearing mice irradiated to the lungs and intestine was reported by Gao et al. [20].

High dose rates of photons can also be produced using light-source synchrotrons, notably synchrotron broad-beam radiation therapy (SBBR) and microbeam radiation therapy (MRT), which generates an array of parallel microbeams, each separated by a few microns, thus spatially separating the delivered dose into ‘peaks’ and ‘valleys’. For the SBBR, one study did not show a FLASH effect (37–41 Gy/s, 4–28 Gy); see Figure 1, ANSTO Rx (2018) [21]. Still, a second study involving mouse-brain irradiation (37 Gy/s, 10 Gy) showed significant cognitive sparing similar to the experience with electron FLASH [22]. The main difference between the two studies was that the second had a vertical beam size that was 20 times smaller than the first.

2.3. FLASH with Proton and Ion Beams

Although pulsed FLASH has been proposed using large synchrotrons and fast extraction, the dose volume remains small and scanning problematic as the beam would likely be re-positioned between spills which makes the treatment time likely incompatible with FLASH conditions. The FLASH output from the 230–250 MeV proton therapy iso-cyclotrons was initially tested with shoot-through (non-degraded) beams achieving FLASH intensities [23,24] but, in recent years, several publications of FLASH studies with spread-out proton Bragg peaks have appeared [16,25–27]. Most of these studies have demonstrated FLASH

effects in small animals but also highlighted the technical challenges that Bragg-peak FLASH proton therapy will face. For a review of the current status and future directions of preclinical proton FLASH research, see Diffenderfer et al. [25]. FLASH research with helium and carbon ions have been confined to in vitro cell survival studies. These studies demonstrated a protection by FLASH irradiation only at very low oxygen concentrations of 1% or less [26,27].

Several clinical studies with protons are underway and the feasibility study “FLASH Radiotherapy for the Treatment of Symptomatic Bone Metastases (FAST-01)” has been completed and reported [8]. Individual RF (MHz) proton bunch structures may be important for proton FLASH (see discussion below); proton RF “bunches” are fractions of a microsecond, and electron RF bunches are fractions of a nanosecond. Further, CW proton beams are “quasi-continuous”, whereas 100–300 Hz electron linacs produce a ~microsecond “macro-pulse” containing many RF bunches and the “instantaneous” dose rate is averaged over the macro-pulse. For proton FLASH, the evidence from the preclinical studies mentioned above shows that a FLASH effect can be achieved despite an orders-of-magnitude-lower dose rate in the proton bunches delivered by iso-cyclotrons as long as the mean dose rate is compatible to those delivered by electron FLASH studies. For pulsed electron beams, the IDR is integrated over the microsecond individual macro-pulse, which repeats at the 100–300 Hz rate of the pulsed linac., as shown in Figure 2. The usually quoted 100 ms treatment time as optimal for electron FLASH may also apply to quasi-continuous proton beams and other quasi-CW FLASH RT sources such as SRF electron linacs.

FLASH beam intensities have been demonstrated using proton-therapy iso-cyclotrons (cyclotrons that produce continuous rather than pulsed beams) and more recently synchro-cyclotrons (cyclotrons that produce pulsed beams of microsecond-length pulses with gaps of milliseconds) [28–30].

With regard to ion therapy, currently, only synchrotrons are available and synchrotrons, even the rapid-cycling 15 Hz ion synchrotron, are not capable of producing the intense ion beams required for FLASH radiotherapy for a clinical application. In addition to providing intense ion beams, FLASH radiotherapy studies need to be extended to incorporate the Bragg peak, range dependencies, and dosimetry into a broader research initiative. Since there are innovative accelerator technologies under development that may provide FLASH intensities for protons and ions, beam conditions can be proposed for the FLASH effect based on the relative biological effects (RBE) and linear energy transfers (LET) between the different particle beams. These extrapolations are presented in Table 2 and compared with a more conventional dose rate and dose fraction.

Most preclinical studies published to date have not been systematically co-ordinated around beam parameters, including the mean and IDR, total dose, pulse structure, fractionation, and radiation type. Although there is a wide range of dose rates, some observations can be made nonetheless, although these may apply only to electron FLASH [12,14,21]. The following itemized list characterizes FLASH from the qualitative and quantitative points of view and raises some questions:

- FLASH effects—general

a. Appear at average dose rates of >30 Gy/s, with the apparent optimal at 100 Gy/s;

b. FLASH effect is likely highly dose-, tissue-, and end-point-dependent.

- Dependence of beam delivery on the beam structure and uniformity in dose deposition

  a. Typical dose delivery time for a consistent (electron) FLASH effect is ~100 ms (best <250 ms);

  b. Most positive FLASH studies used a modified pulsed clinical electron linac with a beam pulse length of ~microseconds and a repetition rate of 100–400 Hz;

  c. Instantaneous (within the pulse) minimum FLASH dose rate is 106 Gy/s (again, a characteristic of clinical electron linacs).

- Dosimetry and treatment-planning questions

  a. Observed volumetric dose-deposition dependence.

  b. Low-dose-rate areas not tolerated during FLASH—toxicity reappears?

  c. Bragg peak and pencil-beam scanning questions: do distal edge and penumbra effects and associated lower-dose rate beam “halos” create a problem?

  d. Can a relatively large target volume be uniformly irradiated by fractionated FLASH-compatible deliveries over a longer time frame?

  e. Instantaneous FLASH dose rate and delivery time for 10 Gy—is it consistent for all radiation types?

3. High-Gradient Ion Linacs for FLASH-RT Developed by Argonne National Laboratory and RadiaBeam

Synchrotrons are used for ion beam therapy, while cyclotrons are mainly used for proton therapy. Until recently, linacs were not seriously considered for ion beam therapy due to the required accelerator length and extended footprint. With the recent developments of high-frequency high-gradient accelerating copper structures, more compact linacs are being proposed for protons and ions. These structures should be capable of delivering FLASH beam intensities.

3.1. Linacs for Ion Beam Therapy

Being a single-pass machine, a pulsed linear accelerator (linac) is capable of adjusting the pulse repetition rate and the beam energy hundreds of times per second (~200 Hz). This much-desired flexibility in beam tuning enables fast and efficient beam scanning to allow 3D dose painting, as well as the real-time image-guided range calculation and targeting of moving targets. By changing the pulse repetition rate, the beam intensity could be adjusted up to 10^9 ions per second (10^{10} for protons), typically needed for therapy. For carbon ions,

the energy could be changed continuously up to the full energy of 430 MeV/u required to penetrate the depth of a human body, which is equivalent to 30 cm of water. In addition, the beam quality from a single-pass full-energy linac is generally better than other systems that may require energy degraders or multi-turn acceleration.

Linacs have already been proposed for proton [31,32] and carbon beam therapy [33], but no all-linac-based facilities exist. This is due to the length and space required for the linac, which has limited its deployment in a hospital or other clinical setting. Using traditional accelerator technology, a linac would be hundreds of meters long, and this is the main reason why synchrotrons are currently dominating the field of ion beam therapy. The beam delivery from a linac will be similar to synchrotron beam delivery through fixed beamlines or gantry systems. However, the superior beam quality of the linac enables much smaller magnets and, therefore, more compact gantries.

3.2. The ACCIL Ion Linac: General and FLASH Capabilities

The advanced compact carbon ion linac (ACCIL) is the most compact full-energy carbon ion linac proposed for therapy [34]. In Europe, there are proposals for a combined cyclotron and linac (cyclinac) and an all-linac for carbon beams [35], in addition to the ongoing LIGHT project for a proton therapy linac [35]. ACCIL is designed to deliver a full energy of 450 MeV/u, which exceeds the maximum energy required for carbon ion therapy. It is also capable of accelerating protons and many other ion beams to the same energy per nucleon. Figure 3 presents a schematic layout of the ACCIL design. The system is about 45 m long but could, in principle, be folded into two 25 m-long sections.

The linac comprises an electron cyclotron resonance ion source, followed by a radio-frequency quadrupole accelerating the carbon beam to 3 MeV/u, which is further accelerated in a drift tube linac (DTL), then in a coupled DTL linac up to 45 MeV/u. The essential features to achieve compactness in the ACCIL design are high-gradient structures, each capable of delivering 50 MV/m, that accelerate the beam to the full energy of 450 MeV/u in ~25 m.

The main advantages of ACCIL are the fast pulse-to-pulse beam energy change and ion beam switching capabilities. Different ion sources could be used in the front end to allow fast beam switching between different ion species. The delivered beam intensity could also be controlled by adjusting the pulse length at the source or changing the pulse repetition rate, typically from 100 to 400 Hz, and R&D for accelerating structures capable of operating at 1000 Hz is ongoing. Ultimately, the tuning flexibility of the ACCIL design will allow fast and effective variable-energy and intensity-modulated multi-ion beam therapy.

ACCIL is capable of accelerating a variety of ion beams from proton to neon, up to a maximum energy of 450 MeV/u. At this energy, ions lighter than carbon, including protons and helium ions, have ranges exceeding the depth of the human body and could therefore be used for imaging such as proton/ion tomography. It is also possible to deliver these beams with lower energies for treatment. Despite having ranges shorter than the human body, ions heavier than carbon, such as oxygen and neon, could still be used for treatment at adjustable energies up to the full linac energy.

As for FLASH, ACCIL's capability is comparable to other existing proton and ion machines [36]. For example, for a proton beam of 230 MeV, losing about half of its energy in the last 10 cm, the energy deposited at 10^{10} protons/s is ~0.16 J/s. The corresponding dose delivered to a spot size of ~5 × 5 mm^2 (2.5 cm^3 beam-stopping volume) is 64 Gy/s, which is well above the FLASH dose requirement of 40 Gy/s. For a carbon ion beam of 430 MeV/u, losing about half of its energy in the last 10 cm, the energy deposited at 10^9 carbon ions/s is ~0.38 J/s, and the corresponding dose delivered to the same stopping volume is 152 Gy/s, which exceeds the FLASH dose requirement and calls for a larger beam spot size. However, to satisfy all cases, for all tumor sizes and beam energies, we would need at least 10 times more particles per second (10^{11} protons/s and 10^{10} carbon ions/s), which is feasible with the ACCIL linac design. In addition, higher repetition rates may be required for faster beam scanning and more flexibility in beam delivery.

3.3. Enabling Technology: Low-Velocity High-Gradient Accelerating Structure Development

ACCIL requires the development of high-gradient structures (~50 MV/m) for ion acceleration with a relative velocity β in the 0.3–0.8 range. This makes the accelerating cells much more compact than β~1 cells built for electrons, especially at the lowest β. A shorter and more compact cell increases the rate of electric breakdowns and makes dissipating the power required for operation at such high gradients challenging. R&D in this field is being pursued at CERN [37], other European institutions, and, more recently, in the US by RadiaBeam and Argonne [38]. In this collaboration, we have developed a β ~0.3 traveling-wave S-band structure (NHS) and demonstrated the 50 MV/m accelerating gradient required for ACCIL [39]; see Figure 4.

This special cavity design for the lowest velocity ions is what distinguishes ACCIL and makes it more compact than other linacs. It allows the transition to high-gradient acceleration to take place at 45 MeV/u, which is much lower than the 70 MeV/u for other linacs. At Argonne, we have also designed and prototyped a cold model of a β ~0.4 annular coupled structure (ACS) [40] as the next accelerating cavity for ACCIL following the NHS; see Figure 5.

3.4. Future Developments for FLASH-RT

In addition to the general development of high-gradient accelerator structures for low-velocity ions, we identify a few areas of R&D of special importance for FLASH-RT [41] with ion beams:

- Investigating and pushing the beam current limit of compact ion linacs;
- Increasing the repetition rate of high-gradient structures;
- Developing RF sources capable of delivering the required high pulsed power.

More importantly, and to enable this technology, establishing a linac-based advanced ion therapy research center in one of the National Labs would be a significant step forward and would allow the following:

- Cancer therapy and radiobiology research with all ion beams up to neon;

- Radiography and tomography with ions lighter than carbon: proton, helium, etc.;
- Real-time MRI guidance during beam delivery, significantly enhancing the outcome of ion beam therapy;
- PET imaging using positron emitters (C-11, N-13, O-15, etc.) produced in the tumor for dose verification;
- FLASH ion therapy (FLASH IT) and other novel approaches.

We mention, in particular, an ACCIL-type linac that could be installed at the existing IPNS site at the Argonne National Lab with the required infrastructure [42], which represents a significant cost saving compared to a greenfield installation [43]. Following the development and commissioning phases, an initial research program including cellular radiobiology and animal therapy could be conducted prior to human therapy and early clinical trials to prepare for FDA approval.

4. Fixed-Field Gradient Accelerators for FLASH-RT

4.1. Scaling Fixed-Field Gradient Accelerator

Fixed-field gradient accelerators (FFGA), previously called fixed-field alternating gradient (FFAG) accelerators, are synchro-cyclotron-style accelerators based on cycled radio-frequency acceleration. Similar to synchro-cyclotrons, FFAGs generally operate at high repetition rates; e.g., the superconducting synchro-cyclotron (S2C2) from IBA (Ion Beam Applications) operates at 1 kHz [44]. Compared to synchro-cyclotrons, a crucial difference of FFGAs is their strong focusing optics (no different from the optical principle of present-day pulsed synchrotrons) which results in a much smaller beam size, as well as the efficient handling of space charge defocusing effects, a concern when aiming at high-charge bunches.

FFGA proton accelerators (aka “scaling FFAG”) were developed at KEK (Kō Enerugī Kasokuki Kenkyu Kikō) in the late 1990s, with a proof-of-principle 500 MeV ring in 1999 [45] and a full-scale 150 MeV ring that provided the first beam in 2005 [46]. Two such rings are in operation in Japan, at Kyushu University (providing the beam for condensed matter research) and at the Kyoto University research reactor (providing the beam for KUCA, an ADS-Reactor Critical Assembly) [46]. These rings have demonstrated a 100 Hz capability based on a single RF system; however, they may even do better as their lattice lends itself to multiple RF systems (in the manner of a folded linac).

Kyoto and Kyushu rings use so-called radial optics, an alternation of positive- and negative- bend radial sector strong focusing dipoles; compact rings, in addition, are obtained using spiral-sector optics. This has been demonstrated by the RACCAM (Recherche en Accelerateurs pour Applications Medicales) project [47], which has produced a design with a multiple-extraction ring (Figure 6), RACCAM-constructed, as a proof of principle, and a strong-focusing spiral sector FFGA dipole [48]; and validated the design with 3D magnetic field measurements which proved that the expected performance was reached [49].

The RACCAM spiral-sector ring design allows a >5 Gy/min dose rate, based on bunchto-voxel delivery to a volume of 1 L (l). The reference volume (1 l) is centered at a 10 cm depth

and comprises 20 × 20 × 20, 5 × 5 × 5 mm^3 voxels [47]. This delivery mode requires a total of 10^{11} protons and, for a uniform, spread-out Bragg peak, 10^9 protons per bunch (ppb) in the most distal layer. Thus, the average dose rate is 5 Gy × l/60 s, i.e., ~0.1 Gy/s over 1 l, which is higher than a typical conventional dose rate but not FLASH-compatible (>40 Gy/s).

Increasing the dose rate could be split between the repetition rate, pushing beyond 100 Hz; bunch charge, pushing beyond 10^9 ppb; and decreasing the irradiated volume. In particular, with the assumption of a 100 Hz repetition rate, a required <200 ms irradiation time imposes ~30 voxels and ~4 mL; current-wise, this is $<I> = 10^9$ ppb × e_c × 100 Hz = 16 nA, where e_c is the elementary charge. An increase of the repetition rate by a factor of 10, to 1 kHz, would allow the irradiation of a ~40 mL volume irradiation in 200 ms; it would also bring the necessary bunch charge for the proper average and IDRs to 4 × 10^9 protons; current-wise, this is ~1 μA.

It can be seen from what precedes that increasing the average current (via repetition rate and/or bunch charge) and instantaneous current (via bunch charge) towards FLASH requirements is challenging but possible. An intermediate option is to consider a smaller target volume, i.e., a few 10s of ml, which would relax the repetition rate and bunch charge constraints.

4.2. Non-scaling FFGA for FLASH

The constraints imposed by the field scaling law are relaxed in the non-scaling variant of the FFGA. Advanced codes and optimizers have been used to stabilize the machine tune consistent with isochronous orbits as in an iso-cyclotron. Isochronous orbits permit the CW and high intensity beam, and the strong-focusing gradients allow long straight sections as with a synchrotron. These straights can be used for high-gradient acceleration and low-loss, variable-energy extraction using large-aperture bump magnets. The system design applied to therapy is described below.

4.2.1. Overview of Principle Design—A compact 250 MeV/nucleon, fixed-magnetic-field turnkey machine has been designed in a racetrack format with a variable-energy continuous-output beam without a degrader, and with low-loss operation. The design is isochronous and produces a continuous beam for the ion species with a charge-to-mass ratio of ½ (H_2^+, D^+, He^{2+}, Li^{3+}, B^{5+}, C^{6+}, N^{7+}, O^{8+}, and Ne^{10+}) and is therefore capable of accelerating all ion species to therapeutic energies. An outer ring can be added to further the energy reach of the ions to the full 430 MeV/nucleon.

Accelerating ions with an approximately constant charge to mass ratio has the advantage of equal beam transmission independent of ion species. Identical operation and extraction are maintained for all the therapeutic ions, including protons (H_2^+), implying a turnkey operation even when switching between ions. Further, the possibility of accelerating and extracting multi-ion composite beams from a mix, or cocktail, of injected ion species (with an effectively equivalent charge-to-mass ratio) is ground-breaking technology. This approach also provides the rapid switching between ion species, a capability based on the <1% rapid adjustments in the RF frequency.

The complete system involves the injector, a pre-accelerator, and the therapy ring—similar to cascade synchrotron systems. To allow variable-energy extraction in a long straight section, the energy range must be restricted in order to extract inner, low-energy orbits using extraction magnets with feasible strengths and in particular apertures. The pre-accelerator extraction energy not only facilitates variable-energy extraction in the higher energy ring, but it can also support an independent beamline for eye treatments and R&D.

4.2.2. The High-Energy Therapeutic Ring—The high-energy ring will be operated from 100 MeV/nucleon up to 250/330 MeV/nucleon to support ion therapy and particle imaging. This energy represents a 15 cm range for carbon and the energy required for the light-ion imaging for pelvic or abdominal scans. The design of the therapeutic ring is a racetrack with opposing 5 m straight sections for RF and injection/extraction (two-fold periodicity). The ring also incorporates a 2 m short straight in the center of each arc for vacuum and diagnostics. Figure 7 shows the layout of the ring and relative size compared to the Heidelberg ion therapy facility which is a slow-cycling synchrotron capable of 430 MeV/nucleon.

Particle tracking has been performed and has a large dynamic aperture with an acceptance >1000 mm-mr (normalized). Arcs can be either SC or normal-conducting. SC extends the energy reach of the extraction system due to a reduced aperture and smaller distance between circulating orbits. However, the orbit separation needs to be studied and optimized for the efficient and clean extraction of different energy orbits and the required acceleration gradient. An acceleration of ~2MeV/turn per nucleon appears to be a maximum step size requirement for longitudinal scanning. The isochronous level of performance in machine design shows less than a percent variation in TOF over an acceleration range from 70 MeV/nucleon to 250 MeV/nucleon.

4.2.3. Variable-Energy Extraction—Extraction is performed in one of the 5 m straight sections and shown in Figure 8. The magnets can be ramped for swept, variable-energy longitudinal scanning or set at a flat top for single energy beam delivery. The field direction is bipolar; the field decreases and flips the sign for maximum inner orbit extraction (blue to red lines). The extraction magnetic fields are limited to ~2.5 T for a ramped system.

4.2.4. Source, LEBT, and RFQ, and Injector—The ion source and beam capture system comprise an electron-cyclotron-resonance (ECR) source coupled to a radio-frequency quadrupole linac (RFQ) through a conventional low-energy beam transport (LEBT) section, as shown in Figure 9. The ion ECR source has one of the highest ionization efficiencies for gaseous elements. An RFQ linac, which uses electrical RF focusing, can capture, auto-bunch, and efficiently accelerate DC (constant current) ion beams directly from the source, achieving energies of several MeV, efficiently replacing complex and lengthy pre-injector elements. The LEBT will consist of an Einzel and solenoid lens system (beam chopping may be required to match RF frequencies between RFQ and injector). In addition, a mixture of ion species can be ionized in ECRs to produce a mixed or ‘cocktail’ of ion beams which potentially can be accelerated in the proposed accelerator system—including all therapeutic ions plus protons in the form of H_2^+—thus combining imaging and therapeutic beams for real-time dosimetry.

An advanced, small-footprint, heavy ion injector iso-cyclotron has been developed for the injector. This novel normal-conducting, separated-sector injector has an optimized strong-focusing field gradient designed to efficiently accelerate light ions with a chargeto-mass near ½ (namely, protons in the form of H_2^+, D^+, He^{2+}, Li^{3+}, B^{5+}, C^{6+}, N^{7+}, O^{8+}, Ne^{10+}, S^{16+}, and Ca^{20+}) scalable up to 70–100 MeV/u [51,52]. Dual, high-gradient, 0.2 MV cavities with a tuning range of ±1% in frequency can accelerate any ion species with this charge to a mass ratio on the 8th harmonic (~45 MHz) with a large turn-to-turn, almost centimeter-level separation—an enabling compact and low-loss extraction technology that eliminates the charge-changing foils (used for injection in ion synchrotrons and extraction in H^- cyclotrons). Low (percent level or less) extraction losses are projected to be compared with the 20–60% (or even higher) losses of proton-therapy CW cyclotrons at extraction.

4.2.5. Outline for the Non-Scaling FFGA for FLASH—A complete CW, variable-energy ion therapy concept has been developed with the pre-accelerator stage design advanced in terms of engineering. Since FLASH intensities have been achieved and the effect observed using proton iso-cyclotrons, this ion therapy complex is FLASH-capable. Further, it has the advantage of supporting essential R&D beyond the shoot-through beams currently available for hadron R&D. In addition to providing intense ion beams, FLASH radiotherapy studies can be extended to incorporate the Bragg peak, range dependencies, and dosimetry into a broader research initiative. The injector and higher-energy therapy accelerator being developed for the National Particle Beam Therapy Center (Waco, TX, USA) will provide the range of ions and intensities, with different LETs and RBEs requested by the medical community in a CW beam format without significant operational modifications and overhead, i.e., a turnkey system. This system represents a significant advance in ion therapy clinical application in addition to playing a critical role in the development of FLASH-RT.

5. FLASH Studies with Laser-Driven Particle Sources Developed at Lawrence Berkeley National Laboratory

5.1. Status of Laser-Driven Particle Sources

Novel laser-driven particle sources are receiving increasing attention due to their potential of providing particle beams for applications on a relatively small footprint and at a potentially lower cost than radio-frequency (RF)-driven accelerators [53,54]. Efficient laser-particle acceleration has become feasible with the advent of ultra-short-pulse high-power lasers enabled by chirped pulse amplification [55], a technology that was awarded the Nobel Prize in Physics in 2018, which yielded peak laser powers exceeding 1 petawatt (PW) [56]. The most prominent acceleration schemes are the laser-wakefield acceleration (LWFA) of electrons [57] and target normal sheath acceleration (TNSA) of protons and ions [58]. LWFA is conducted with gas targets that are quickly ionized by the leading laser pulse edge, followed by the formation of collective plasma oscillations in the wake of the pulse as it propagates through the transparent plasma. Free electrons are accelerated up to several GeV energies in dynamic electric fields associated with the resulting plasma wave [59,60]. If optimized, monoenergetic electron bunches with an nC charge can be generated [61]. At the time of writing, the LWFA electron energy record was held by Lawrence Berkeley

National Laboratory, with 8 GeV and few pC charge [62]. LWFA sources can be used to drive compact light sources from the high-field THz [63] over the high-brightness X-ray [64] to the gamma-ray range [65].

TNSA is generally pursued with solid targets, most commonly in the form of few μm-thick metal or plastic foils that are ionized by the lead edge of the laser pulse. The laser peak intensity interacts with free electrons in a preformed plasma layer at the target surface. Electrons gain energy in the laser field, circulate through the target bulk, and expand beyond the predominantly fixed ion distribution at the target surfaces. The resulting quasi-static charge separation fields are in the order of TV/m and lead to the acceleration of protons and ions to >10 MeV energies, emitted along the target normal with a beam divergence of roughly ± 20° [23,24,66,67]. The generated proton beams are of high flux (up to 10^{13} particles per pulse [68]) and feature broad exponential energy spectra up to the characteristic cutoff energy, approaching 100 MeV [69–72].

At the current PW laser pulse repetition rates of at most 1–10 Hz, directing laser-driven (LD) particle beams to biological samples results in a moderate mean dose rate. However, due to their generation mechanism, resulting in ultra-short particle pulse lengths of less than a picosecond at the source, LD particle beams naturally feature ultra-high IDR, exceeding 10^9 Gy/s. This IDR is several orders of magnitude higher than dose rates typically delivered with RF-driven accelerator technology [73].

5.2. Laser-Driven Particle Sources for Preclinical Radiobiological Studies of the FLASH Effect

Laser-driven (LD) particle sources may soon become adequate complements to RF-driven accelerators for basic radiobiological research of the FLASH effect [74]. Access to conventional experimental and medical machines has been rather limited for this type of research [75] while the steady increase in the available compact LD particle sources has already started to open up new experimental options for systematic radiobiological studies.

The majority of radiobiological studies with LD particle sources has been conducted in view of potential future applications in radiotherapy, in particular with protons and heavier ions. As such, an appreciable number of in vitro studies and one in vivo study [76] have been conducted to investigate the radiobiological effectiveness of LD protons [77–88]. Fewer radiobiological studies were so far conducted with LD electrons [89–94]. The only in vivo study found no difference in tumor-growth delay when comparing LD electrons and RF accelerated electrons [91]. The proposal of using very-high-energy electrons (VHEE), with energies in the range of 150–250 MeV for radiotherapy [95], has sparked renewed interest in the dosimetric properties and the potential for new radiotherapy protocols using compact LWFA electron sources [96–98]. So far, no differential sparing effect of normal tissue was reported from radiobiological studies with LWFA electrons.

While the dose rate was not always specified in publications, it can be assumed that samples were irradiated at ultra-high IDR due to the LD particle acceleration mechanisms, as mentioned above. So far, the majority of radiobiological studies with LD particle beams were conducted using in vitro cell cultures and at atmospheric ~20% oxygen levels.

Magnetic transport beamlines have been implemented at a few laser facilities to transport LD protons to a dedicated sample site and apply a three-dimensional dose profile for in vivo studies with small animals, for which tumor models have been developed [99–102].

In a preliminary study at the 40-Joule BELLA petawatt laser proton beamline, it was demonstrated for the first time that LD protons delivered at ultra-high IDR can indeed induce the differential sparing of normal versus tumor cells in vitro for total doses ≥7 Gy [88]. In that study, normal and tumor prostate cells in 1 cm-diameter custom cell cartridges were irradiated with LD protons of 2–8 MeV at an IDR of 10^7 Gy/s. After acceleration from a tape-drive target, the proton bunch was transported with a compact active plasma lens beamline [103] to the cell sample site located outside the vacuum chamber (Figure 10a). An integrating current transformer (ICT) was implemented for the online beam charge measurements. The dosimetry was performed with calibrated radiochromic films attached to every cell sample. With 1 Gy applied per laser shot, total dose values up to >30 Gy were accumulated by operating the LD proton beamline at 0.2 Hz. A significant sparing of normal prostate cells compared to prostate tumor cells was observed after irradiation with LD protons (Figure 10b). The main proton beam parameters for this study are summarized in Table 3.

Reference irradiations with X-rays at clinical dose rates did not show a similarly differential radiosensitivity. It should be pointed out that the generation of LD proton beams in the energy range sufficient for this type of study does not require a PW laser system but was demonstrated in numerous experiments at 100 TW-class laser systems [70,71].

5.3. Potential of Laser-Driven Particle Sources for FLASH Radiation Therapy

Preliminary in vitro experiments with LD ion sources have shown promise for FLASH radiotherapy [88]. However, stringent requirements concerning combined key beam parameters such as proton energy (up to 250 MeV), numbers of protons per bunch (10^9), stability and control of energy and proton numbers from shot to shot (<few percent variation), and repetition rate (>10 Hz) are yet to be experimentally demonstrated [104].

Currently, the primary challenge for the field of laser-ion acceleration is reaching clinically relevant particle energies. So far, peak LD proton energies achieved in experiments are approaching 100 MeV [72], which is well below energies necessary for clinically relevant penetration depths of >30 cm in humans [74]. In terms of ongoing efforts to develop a high repetition rate, several PW-class lasers can theoretically overcome this challenge when combined with improved gantry designs and treatment-planning strategies specific to LD particle sources [105,106]. Currently, no unified reference dosimetry protocol exists for LD particle beams, which are unique in their ultra-high IDR and, in the case of ions, broad energy spectra. However, innovative dosimetry methods for radiobiological studies with LD proton sources have been developed that use online, minimally invasive, relative dose detectors, e.g., thin transmission ionization chambers, corrected for recombination effects [107], or integrating current transformers [108] that can be cross-referenced with independent absolute dosimetry methods such as radiochromic film [109] or Faraday cups [110]. These have enabled in situ dose-controlled LD proton irradiations of biological cell samples at a relative dose uncertainty below 10% [111].

Advances in laser technology are expected to deliver higher LD proton and ion energies because experiments and simulations have shown a consistent increase of maximum particle energies with laser pulse energy, power, or intensity [70,71]. At the same time, theory and simulations predict higher proton and ion energies when harnessing advanced acceleration regimes including, for example, radiation pressure acceleration [112], magnetic vortex acceleration [113], and shock acceleration [114].

Given that the aforementioned ion-source requirements are met, designing a hypothetical compact LD FLASH radiotherapy machine requires careful consideration of not only the laser particle source but also the treatment beam delivery system that needs to reliably shape a six-dimensional dose profile matching the tumor profile, of which first designs exist [105]. As such, even after optimizing the LD particle sources for the footprint, which, on the laser side, may come naturally with advances in laser technology, it remains to be seen whether they can compete in compactness and cost with emerging conventional proton therapy machines, e.g., compact solutions by Mevion, IBA, Hitachi, and others, which have seen significant developments in recent years to reduce their footprint and cost [104]. However, these machines are typically not able to deliver comparable IDR as LD proton sources, and, so far, no such compact machines exist for heavier ions, which are automatically accelerated alongside protons in LD ion accelerators.

With the current interest in using VHEE for radiotherapy, LWFA may well offer the most promising method for compact and affordable VHEE medical machines that can operate in the ultra-high IDR regime [54]. While the necessary electron energies are readily generated in a well-controlled laboratory setting, the long-term source stability and reproducibility require further improvement. Moreover, current limitations to the achievable mean dose rate due to lower repetition rates compared to RF-driven accelerators, in combination with a lower, less-localized energy deposition compared to ions, need to be addressed. Current efforts towards high-average-power, Joule-class kHz laser systems may provide solutions for some of these issues [115].

5.4. Outlook for Laser-Driven FLASH

To summarize, current LD particle-source parameters are well below the requirements for their use as an alternative medical FLASH radiotherapy modality. However, their comparatively low cost and compact nature has earned LD particle sources increasing attention and the differential normal vs. tumor cell sparing in vitro under LD proton irradiation was recently demonstrated [88]. Therefore, LD particle sources could soon complement conventional accelerators to increase and democratize access to particle sources for preclinical radiobiological research. This real-world application can serve as a stepping stone to further advance LD particle sources to the necessary capabilities to provide particle beams for FLASH radiotherapy.

6. High-Peak-Current Linear Induction Accelerator (LIA) for FLASH-RT Developed at Lawrence Livermore National Laboratory

Meeting the requirements for reproducible FLASH effects of $>1.8 \times 10^5$ Gy/s IDR with an overall irradiation time <200 ms (>40 Gy/s average dose rate for healthy tissue sparing) using deep-penetrating MV bremsstrahlung requires tens of amperes of pulsed electron beams at a high pulse-repetition frequency (PRF) [2,116]. These dose rate criteria must not only be met in the core of the irradiated volume but in the whole of the volume as well (i.e., beam penumbra and exit edge) [21].

The pulsed-power-based linear induction accelerator (LIA) using a multilayered bremsstrahlung conversion target meets these demanding requirements. Complementary irradiation sources from the same accelerator structure ensure that the whole of the irradiated volume is above the FLASH threshold. The LIA acceleration technique stores energy during the interpulse time and then discharges it in a short, 10s-of-nanoseconds pulse to achieve extremely high IDR. This method is a direct acceleration technique using *induction* and does not require RF or microwave generation as an intermediate step. When operated at a clinician-specified kilohertz PRF, equivalent dose rates exceeding the healthy-tissue-sparing thresholds can be easily achieved, and the concentration of specific radicals, thought to play a role in the FLASH process, can be manipulated (see, for instance, [117]). Using active control of the individual pulses ensures safe dosing. While not widely known to the medical community, existing systems have been used as 10s of MeV, kiloampere electron, or ampere level hadron sources since the 1960s [118].

A key demonstrated capability of the technology is that the beam pipe can be made arbitrarily large without affecting the acceleration gradient [119,120]. This property enables independently controllable, multibeam acceleration through a single accelerator structure for complimentary irradiation. While the gradient of older induction linacs is low (<1 MV/m for 50–70 ns pulses), modern approaches enable 5–10 MV/m gradients. Thus, a 16 MeV system with four to eight or more individual beams with variable energy and pulse rate would fit in a clinic-sized vault of ~100 m^3.

Figure 11 depicts an artist’s conception of a four-beam system; added beams are easily implemented [121]. The accelerator cells can be seen beyond the patient and patient couch. Four separate electron beams are being accelerated away from the patient, captured, and then bent 180° with two 90° dipoles. Solenoid transport is then used to return the beam alongside the patient, and a third 90° dipole directs the beam to a target where it is converted to bremsstrahlung. Multi-leaf collimators (MLC) can be used in this region for conformal therapy.

6.1. Illustrative Measurements from LIAs for FLASH-RT

Bremsstrahlung generated by an LIA provides a broad-area, deep-penetrating, and high-dose-rate capability. This unique capability results from the elimination of the resonant structures characteristic of the majority of acceleration techniques. Such structures are prone to pulse-shortening-beam instabilities and also the degradation of the acceleration

gradient when beam currents approach one ampere [122–124]. We present measurements on the FLASH X-ray (FXR) accelerator used to accelerate electrons to 17 MeV and briefly describe the Experimental Test Accelerator-II (ETA-II) with a nominal output energy of 6.5 MeV but at kilohertz PRF [125–127].

The FXR geometry and measurements are shown in Figure 12. This particular arrangement consisted of the bremsstrahlung converter target, a fast CVD diamond FLASH dose detector, an 8 cm-thick low-energy filter, and either a thermoluminescent (TLD) or film detector at 1–2 m [127]. The 90–100% flat field is approximately 21 cm in diameter at 1 m. This measurement corresponds to an approximately 350 cm^2 area demonstrating that FLASH levels can be maintained in the totality of an irradiated volume. We observe a *single-shot, stable* dose of approximately 4.19 Gy with $1\sigma \approx 0.16$ or a 3.9% variation. This value corresponds to an IDR of approximately 6×10^7 Gy/s.

On ETA-II, a 5 kHz PRF has been demonstrated. This system also produced highly stable electron beams with a less-than-1% energy variation, millimeter spot size, and submillimeter spot motion. Initial use of the accelerator was in conjunction with a wiggler to generate electromagnetic energy at 2 GW and 140 GHz mm-wave energy for fusion research studies [128].

6.2. Meeting the Criteria for FLASH-RT

To ensure that both the periphery and exit dose rate were above the healthy-tissue-sparing threshold to minimize toxicity, we performed calculations assuming a minimum of four separate sources placed symmetrically around a water phantom volume approximating the average human torso's 16 cm radius [21,129]. Each source provides 25 Gy/s at 1 m using a total beam current of 25 A; details are provided elsewhere [121]. This configuration achieved 50% beyond the required average healthy-tissue-sparing dose rate, or about 60 Gy/s throughout most of the volume. By contrast, a single source at the same level achieved the healthy-tissue-sparing dose rate >40 Gy/s nearest the source, but about 25% of the volume is below that dose rate, potentially inducing toxicity. Noting that the total beam current for LIAs typically exceeds 1 kA, the current can be used as a free parameter for an increased dose rate.

The model assumed a single LIA to accelerate separate beamlets in an approximately 14 cm-diameter beam pipe. While four beams are shown, eight or more can be easily implemented in an actual system. Beam transport is managed through the accelerator with solenoid coils and integrated steering similar to the FXR geometry [125]. The added steering capability allows generating oblique rays for a closer approximation of multibeam conformal therapy. Based on the model, at 16 MeV, the system would be approximately 3.2 m long (Figure 11), delivering a uniform average dose rate of 60 Gy/s at a beam current of 25 A at 10 kHz PRF.

7. High-Current Electron Linear Accelerator for X-ray FLASH-RT Developed by RadiaBeam and UCLA

7.1. X-ray FLASH-RT

An attractive tool for delivering FLASH-RT could be a FLASH-capable X-ray system. More than 80% of all radiotherapy is delivered with X-rays [130]. They are the most versatile form of radiation therapy and the most cost-effective. Unfortunately, the physical process for generating X-rays is not very efficient [131]; therefore, a high-power accelerator is needed for X-ray FLASH-RT [132]. Furthermore, one would still like to achieve as much conformality as possible. Conformality, combined with the healthy-tissue-sparing FLASH effect, promises to dramatically improve patient outcomes [5].

Considering the inevitable reduction in effective dose rate with the intensity modulation and transmission through small apertures, a linac that can deliver 100 Gy in one second or faster is challenging but not impossible. Conventional 6 MV medical linacs produce a flattening filter-free dose rate of around 0.2 Gy/s at one meter from the X-ray target—three orders of magnitude too low. However, they are on the low end of the spectrum of linac powers [133]. A typical medical linac has a beam power on the order of 1 kW. In comparison, industrial accelerators for sterilizing food and medical products can achieve beam powers of several hundred kW [134].

Another factor that allows for the improvement in the dose rate is increasing the beam energy. The conversion efficiency from electron beam power to X-ray power scales approximately with E^3, so a small increase in energy can make a big difference in X-ray intensity. The higher X-ray energy also allows greater penetration. However, there are two major downsides to higher photon energies: larger lateral penumbra (a measure of the fuzziness at the edge of the beam) and greater neutron production (which causes activation and an unwanted dose to the patient and the environment). Photon energies up to 20 MV are commonly used in RT. We consider 10–18 MV to be optimal for achieving a high dose rate while limiting the negative factors.

One could also consider reducing the distance from the source to the target. However, this can only be done to a certain point without sacrificing useability. Achieving good conformality requires placing one or more collimators between the beam source and the patient. Along with the pure physical limitations on fitting the equipment around the patient, this limits the source-to-surface distance (SSD) to 80 cm at the smallest.

7.2. New Technology for X-ray FLASH-RT

RadiaBeam and UCLA are working on a solution for X-ray FLASH therapy that takes advantage of a single linac based on already-demonstrated technology and an innovative yet straightforward method for intensity modulation [135]. The major innovation of the proposed project is the development of the rotational direct aperture optimization with a decoupled (ROAD) multi-leaf collimator (MLC) ring [136]. Intensity modulation has been the key driver in improved patient outcomes in RT over the past three decades, but there has been no solution to do this in the short time required by FLASH. With ROAD, the linac

pulses are timed to align with a counter-rotating ring of 75 pre-shaped MLC apertures. As the linac and MLC rings rotate in opposite directions at 60 rpm, 150 modulated beams are delivered in 1 s, each delivering up to 0.7 Gy to the tumor. ROAD can achieve physical dose conformality superior to state-of-the-art VMAT plans free from the MLC mechanical limitation, yet with the added benefit of the FLASH effect. Figure 13 shows a model of the proposed ROAD-FLASH system [137].

The linac (see Table 4 for a summary of parameters) consists of a 1.3 A, 140 kV electron gun, prebuncher [138], and two traveling wave linac sections powered by a commercially available 20 MW L-band klystron with 167 μs pulses at 150 Hz, to bring an 8.14 mA average current electron beam to 18 MeV. Assuming a dose conversion factor of 2000 Gy/min/mA at 18 MeV, such a linac will be able to provide an uncollimated dose rate of 271 Gy/s at 1 m (8.14 mA × $2{\cdot}10^3$/60 Gy/s/mA), which is equivalent to a ~100 Gy/s collimated dose at 80 cm, assuming a ~25% dose delivery efficiency [139]. The beam is transported through a rotary vacuum joint into a rotating magnetic gantry that brings the beam to a rotating X-ray target directed at the patient.

Figure 14 shows the proposed FLASH delivery using the ROAD method. There are a total of 75 MLC modules on a ring that is separate from the X-ray source. The X-ray pulses are triggered when the source is sequentially aligned with the MLC apertures. Counter-rotating the MLC ring allows more aperture shapes to be programmed for a further improved physical dose conformity.

With an increasing understanding of the underlying FLASH mechanism, it is necessary to further quantify the FLASH effect at the treatment-planning stage as part of the inverse optimization goal. The feasibility has been demonstrated for the simultaneous dose and dose rate optimization (SDDRO) with protons [140] and X-ray ROAD FLASH [136]. In the latter, the hypothesized oxygen depletion effect was parameterized into the planning system to show a larger FLASH effect for normal tissue sparing with larger individual pulses. The information will guide the design of high-output and FLASH-ready linear accelerators.

8. Accelerator-Based Technology Developed at SLAC National Accelerator Laboratory and Stanford University

8.1. X-ray FLASH-RT with the PHASER

The inherent inefficiency of producing therapeutic X-rays through bremsstrahlung radiation from an electron beam hitting a target contributes to the challenge of achieving FLASH dose rates with conventional photon radiotherapy. Another critical factor constraining the treatment time in a conventional radiotherapy device is the mechanical motion of the gantry and multi-leaf collimator. The PHASER program for pluridirectional high-energy agile scanning electronic radiotherapy, led by the SLAC National Accelerator Laboratory and Stanford Medical School, seeks to eliminate gantry and collimator motion while achieving the FLASH dose rate through a system of 16 linacs arrayed around the patient, as shown in Figure 15, and electronic scanning of the bremsstrahlung source coupled with a beamlet-based collimator array [141]. This design enables multiple angles of approach, as needed

for intensity-modulated conformal radiation therapy. The PHASER program is intended to increase the therapeutic index of radiotherapy through highly conformal image-guided FLASH treatments and improve the accessibility of state-of-the-art FLASH-capable medical equipment through the implementation of a compact and economical design.

PHASER seeks to achieve FLASH capability by producing a >400-fold increase in the average beam current compared to conventional 10 MV photon therapy systems with a typical dose rate of 10 Gy/min. The linac structure will rely on a distributed coupling topology to improve the power efficiency [142], allowing the system to take advantage of a network of 16 compact “klystrinos”, each producing a peak power of around 330 kW. The R&D from the initial PHASER program has laid the groundwork for extending the design concept to a very-high-energy electron (VHEE) therapy system, treating directly with ≥100 MeV electrons without X-ray conversion [143], as well as eventually with protons.

8.2. Very-High-Energy Electron (VHEE) FLASH-RT

Very-high-energy electron (VHEE) radiotherapy is a key area of opportunity to apply technology developed for the particle physics community to the new field of FLASH-RT. Direct use of an electron beam for radiotherapy provides one of the most readily scalable paths to achieve FLASH dose rates, as apparent in the existing body of experimental evidence for FLASH that has been predominantly performed with direct electron beams [1,14,144,145]. Existing facilities have been modified for FLASH radiotherapy experiments [137,146,147] and commercial systems such as the Oriatron eRT6 from PMB-Alcen [148], Kinetron from CGRMeV [149], Novac7 from Sordina [150], and the Mobetron from IntraOp [151] have been employed for FLASH capability at sub-10 MeV electron energies. While clinical and pre-clinical commercial devices proceed with development to provide ultra-high-dose-rate direct electron therapy [152–155], treatment of superficial tumors in human patients has already begun [2].

The key technological advance where active research is needed concerns the development of medical accelerators that can reach the high beam energies required for the treatment of deep-seated tumors throughout the body. The electron beam energy determines the penetration depth, with a 100 MeV beam reaching a depth of about 40 cm, sufficient to cover almost all deep-seated tumors [156,157]. VHEE therapy has yet to be realized in a clinical setting, because the existing equipment lacks the capability to reach these beam energies. The maximum energy obtained for direct electron FLASH-RT thus far has been only 20 MeV, using a modified Varian Clinac [144,145]. The size and power requirements to simply extend this structure to produce 100 MeV beams would be prohibitive for clinical use. The high beam energies used for VHEE treatments will also impose additional shielding requirements on the treatment facility. Treatment-planning studies using Monte Carlo simulations indicate that a dose rate of approximately 2×10^4 Gy/s can be achieved per milliamp of average beam current over a 10 cm by 10 cm field size.

Current RF-driven linear accelerator research programs aimed at meeting the demand for VHEE capability have primarily focused on advanced, normal-conducting, high-gradient accelerator RF technology. A CHUV-CERN collaboration to build the deep electron FLASH therapy (DEFT) facility plans to combine an X-band linac design developed through CLIC

research with an S-band photoinjector [158]. Designs for a VHEE system at the PRAE accelerator utilize an S-band linac in addition to an S-band photoinjector, prioritizing linac performance reliability [159]. The implementation of a photoinjector with a medical linac has yet to be demonstrated, but the strategy of utilizing a photoinjector has already been proposed as an opportunity to harness the speed and flexibility of laser-based beam-shaping techniques [141].

While the proposed DEFT facility will occupy a length of around ten meters, an R&D effort currently underway at the SLAC National Accelerator Laboratory seeks to reach an even more compact VHEE system using a cryogenic X-band accelerator to achieve VHEE beam energies in only one meter. This approach harnesses the enhanced efficiency and higher gradient obtainable in a distributed coupling linac, combined with the improved scaling at cryogenic temperatures [142] to reach the target gradient of 100 MeV/m, already demonstrated in previous experiments at SLAC using a cryogenic X-band structure at the X-band test area (XTA), see Figure 16 [143].

A key aspect of the proposed VHEE system is the reliance on a commercial RF source, limiting the initial peak power to roughly 6 MW, but ensuring the final product can be widely adopted for commercial use. Advances in both the distributed coupling design and cryogenic operation of the normal conducting structure are necessary to maximize the power efficiency of the linac, allowing SLAC's one-meter X-band structure to reach a gradient of 100 MeV/m while using a peak power of only 20 MW. A preliminary design of the cryogenic X-band linac is shown in Figure 17.

The SLAC system will rely on RF pulse compression to achieve a 20 MW peak power using the initial 6 MW pulse produced by the commercial klystron. RF pulse compression is a mature technology that has been used extensively for large-scale accelerator applications to reconcile the need for short high-peak-power pulses with a cost-efficient long-pulse, lowpower sources [160–162]. Recent advances in RF compressor technology have opened the door to compact structures that could dramatically reduce the system footprint while maintaining the capability to produce a four-fold pulse compression and isolate the source from the reflected RF signal from the cavities [163,164]. The SLAC VHEE program investigates multiple cavity designs, such as the spherical cavity in Ref. [163], focusing on structures designed for high intrinsic quality factors, Q0 up to 400,000, and high coupling factors, β up to 10. Active research in this area will continue to benefit efforts to design a new generation of compact, cost-efficient medical accelerators and the broader accelerator community that relies on pulse compressors to supply the peak powers needed for high-gradient operation.

Proposed programs such as the Cool Copper Collider (C^3) proposal [165] to realize a e^+e^- collider for the study of the Higgs boson offer an exciting opportunity for synergistic research efforts on accelerator technologies, from the distributed coupling linac to the pulse compression system, which could enhance power efficiency for a single compact cancer therapy system up to a large-scale facility such as C^3. In each case, the same underlying techniques are used to push the limits on achievable accelerating gradients with a cost-efficient system. Research from a C^3 linac R&D effort [166] would provide insight

into features needed for a high-gradient VHEE system and vice versa, including stringent performance reliability criteria optimized for a substantial beam current under cryogenic operating conditions.

The fabrication of SLAC's X-band distributed coupling linac for VHEE will rely on a split-block approach which allows significant flexibility for the CNC machining of the linac cavities and power coupling manifold into the copper slabs. This flexibility is critical for implementing a 135° phase advance linac design which further enhances the power efficiency, increasing the shunt impedance by nearly 10% compared to the π-mode. On-going collaboration with industry partners will facilitate the transition of SLAC's prototype VHEE system into modular industrialized equipment. Mass production will be an important feature not only for commercialization generally, but also for achieving FLASH capability with the VHEE system. In order to eliminate gantry motion and reach an ultra-high dose rate, the proposed FLASH VHEE system utilizes an array of 16 linacs, in the same architecture as the PHASER system for photon therapy [141].

VHEE beam energies as high as 250 MeV could be needed for treatment scenarios that use advanced techniques such as spatially fractionated radiotherapy in combination with FLASH dose rates [167]. The demand for equipment that can deliver these beam energies on the meter scale has motivated a search for technology that can provide gradients exceeding 100 MeV/m at the FLASH dose rate. Accelerators operating at even higher frequencies than X-band, up into the mm-wave regime, offer an opportunity to provide VHEE FLASH-RT with unprecedented compactness. Efforts are already underway at the SLAC National Accelerator Laboratory to apply recent advances in mm-wave linac fabrication and high-power testing (Figure 18) to the design of a VHEE accelerator operating at 94 GHz [168].

The mm-wave and THz regime has long been frustratingly inaccessible for accelerator applications due to the absence of high-power sources and the challenges of implementing these small-scale structures. Motivated by the potential advantages of high-frequency high-gradient accelerators to explore the Energy Frontier, research has been conducted at SLAC on the fabrication of mm-wave accelerators [169] as well as methods of powering these structures and the physics of breakdown at these high frequencies [170]. New research is exploring the benefits of applying high-gradient techniques such as distributed coupling and cryogenic operation in the mm-wave regime [168,171]. These features offer the possibility for extremely power-efficient structures that could reach gradients of hundreds of MeV per meter. To power these structures, SLAC has partnered with the Air Force Research Laboratory to investigate active pulse compression at mm-wave frequencies, overcoming the limitations of the low peak power available from commercial sources using techniques developed for nanosecond RF-power switching [172,173]. Active R&D is needed to push these structures beyond the few-cell prototypes that have undergone high-power tests to a full-scale system with demonstrated beam acceleration. A critical area of research, particularly in the pursuit of FLASH dose rates, will be the design of an electron gun compatible with these mm-wave structures [174].

8.3. Fast 3D High-Speed Beam Scanner for Hadron FLASH-RT

Proton therapy, and hadron therapy in general, allows potentially far greater doseshaping control than conventional photon therapy or VHEE through the energy-dependent Bragg peak, which determines the depth at which the peak dose will be delivered. Proton cyclotron facilities for cancer therapy routinely alter the proton beam energy used in treatment by passing the beam through a so-called range shifter, a physical barrier of material, typically plastic, which reduces the beam energy according to the thickness of the plate. While the strategy is a reliable and robust method for changing the beam energy, the process of switching between range-shifter settings is time-consuming, on the order of a second [175] when compared to the desired time scale of a total FLASH treatment that is a few hundred milliseconds, and also degrades the lateral penumbra of the beam. Synchrotron facilities, used for both proton and carbon cancer treatment, can change the beam energy by adjusting the acceleration cycling settings, avoiding the mechanical motion of a range shifter, but face challenges to achieving the FLASH dose rate. The demand for high-speed changes to the beam energy presents a tantalizing opportunity to apply accelerator technology in which RF-driven energy modulation could accomplish the same objective as the range shifter with changes on the sub-μs scale.

This research thrust has already gained traction in a program at the SLAC National Accelerator Laboratory to develop a 3D high-speed beam scanner for hadron therapy. The objectives of this project are to design and demonstrate the component technology needed to modulate the beam energy and transverse steering, sufficient to cover a 4 L volume at a FLASH dose rate. The energy modulator design builds on research concepts developed at SLAC for high-energy physics applications, taking the high gradient capability of a distributed coupling S-band structure and using it to reach a +/−30 MeV beam energy, equivalent to a range of 15 cm in treatment depth, in a one-meter structure [32].

SLAC’s hadron-scanning program tackles not only the challenge of RF-driven energy modulation but also transverse steering. Unlike conventional photon-based radiotherapy, VHEE and proton therapy allow for pencil-beam scanning, which takes advantage of the Lorentz force to steer the charged particle trajectories. Thus far, transverse pencil-beam scanning for protons has been routinely accomplished using electromagnets, which allow the beam to cover a large treatment field on the order of 30 cm by 40 cm at the patient isocenter [175,176]. This technique offers valuable flexibility in terms of coverage area with minimal beam distortion and, while not as fast as an RF-driven process, is compatible with the timescale of the FLASH dose delivery. Changes to the beam position can be accomplished on the scale of a few hundred microseconds [175]. Varian has already announced FLASH capability with their existing proton therapy equipment and has actively invested in FLASH therapy research through the FlashForward™ Consortium [177].

These developments suggest that proton therapy will likely be one of the leading modalities for FLASH treatment in the near future. The ultrafast 3D beam shaping for hadron therapy championed by the SLAC-led collaboration on RF-driven beam manipulation offers an opportunity for the accelerator technology of the high-energy physics community to revolutionize the speed and flexibility of proton therapy equipment. SLAC’s proton deflector cavity, shown in Figure 19, is a prime example, taking inspiration from CERN’s crab cavity

research for beam steering [178] and optimizing a new cavity design for sub-relativistic protons [179]. The initial design for the SLAC 3D-scanning system utilizes a few-cell deflector structure, with cavities oriented orthogonally for the full range of transverse motion. The angular kick provided by the RF-driven deflector is enhanced by a set of static permanent magnet quadrupoles (PMQ). The effect of the PMQs will be to defocus in one plane and overfocus in the other. By compensating with the magnitude of the kick supplied by the deflector structure in each direction, this focusing action can be optimized for the maximum treatment area, covering around 15 cm × 22 cm for a proton beam energy of 200 MeV. This RF-driven approach to the proton beam modulation eliminates all mechanical motion and allows for ultra-fast switching between different energies and lateral positions.

The initial SLAC research has focused on the design and demonstration of prototypes of both the energy modulator and deflector, with high-power testing underway at SLAC's facilities. In order to realize this technology in clinical settings, R&D will be needed to build the full-scale accelerator structures and conduct testing with a proton beam. SLAC has partnered with Electron Energy Corporation (EEC) to investigate designs for the PMQ system used to enhance the treatment field covered by the SLAC RF deflector. EEC's research on cryogenic PMQ designs offers unique advantages in terms of flexibility and performance reliability over a range of cryogenic temperatures, with applications not only to potential proton therapy equipment but also to programs pushing the Energy Frontier such as the C^3 proposal to develop a e^+e^- collider for the study of the Higgs boson [180].

9. Conclusions

FLASH radiation therapy (FLASH-RT) is the next frontier in radiation therapy for cancer. The initial preclinical and clinical research results look very promising. This research thrust has already gained traction in programs at the National Accelerator Laboratories and leading universities in the United States to develop new compact solutions for FLASHdose-rate-capable machines delivering X-rays, electrons, protons, and ions. Investment in R&D and the close collaboration with the industry and academic medical institutions will be needed to realize this new technology in clinical settings.

Funding:

The work on ACCIL was supported in part by the U.S. Department of Energy, Office of High Energy AQ:2 Physics, through SBIR/STTR under Grant DE-SC0015717, and in part by the AQ:3 Accelerator Stewardship under Grant 0000219678. The work on non-scaling FFGA was partially supported by the U.S. Department of Energy under SBIR Grant DE-SC0020009. The PHASER research is supported by the NIH/NCI Grant 2R44CA217607, Stanford University Department of Radiation Oncology, and philanthropic donors to the Stanford University Department of Radiation Oncology. The ROAD project is funded by the National Institutes of Health (NIH), award number NIH R01CA255432. The LIA work was performed under the auspices of the U.S. Department of Energy by Lawrence Livermore National Laboratory under Contract DE-AC52–07NA27344. Work performed by Opcondys, Inc. was funded separately by the United States Government under ARPAE (Contract No. DE-AR0000907), the National Science Foundation (Grant No. 1519964), and the California Energy Commission CalSEED Program (Grant No. 17–01-03). Emma Snively and the mm-wave VHEE development at SLAC were supported by the Department of Energy, Laboratory Directed Research and Development program at SLAC National Accelerator Laboratory, under Contract DE-AC02–76SF00515, and the LaserNetUS. Authors from LBNL acknowledge support from the Laboratory Directed Research and Development (LDRD) funding from LBNL provided by the Director, the U.S. Department of Energy Office of Science Offices of High Energy Physics and Fusion Energy Sciences, under Contract No. DE-AC02–05CH11231, and the LaserNetUS.

Conflicts of Interest:

Billy W. Loo Jr. is an employee of Stanford University School of Medicine. Dr. Billy W. Loo Jr. has received research support from Varian Medical Systems. He is a co-founder and board member of TibaRay. Reinhard Schulte is employed by Loma Linda University, School of Medicine. Dr. Schulte has received research funding by Grant R44CA257178 “Ultrafast and Precise External Beam Monitor for FLASH and Other Advanced Radiation Therapy Modalities” from the National Cancer Institute awarded to Peter Friedman (PI), Integrated Sensors, LLC. The funder had no role in the design of the study; in the collection, analysis, or interpretation of data; in the writing of the manuscript; or in the decision to publish the results. The United States Government has rights to patents pursuant to Contract No. DE-AC52–07NA27344 between the United States Department of Energy and Lawrence Livermore National Security, LLC for the operation of Lawrence Livermore National Laboratory. For SES, Opcondys, Inc. is a for-profit company and may profit from the technologies described in this paper.

Data Availability Statement:

Not applicable.

References

1. Favaudon V; Caplier L; Monceau V; Pouzoulet F; Sayarath M; Fouillade C; Poupon M-F; Brito I; Hupé P; Bourhis J; et al. Ultrahigh dose-rate FLASH irradiation increases the differential response between normal and tumor tissue in mice. Sci. Transl. Med 2014, 6, 245ra93.
2. Bourhis J; Sozzi WJ; Jorge PG; Gaide O; Bailat C; Duclos F; Patin D; Ozsahin M; Bochud F; Germond J-F; et al. Treatment of a first patient with FLASH-radiotherapy. Radiother. Oncol 2019, 139, 18–22. [PubMed: 31303340]
3. Gaide O; Herrera F; Sozzi WJ; Gonçalves Jorge P; Kinj R; Bailat C; Duclos F; Bochud F; Germond J-F; Gondré M; et al. Comparison of ultra-high versus conventional dose rate radiotherapy in a patient with cutaneous lymphoma. Radiother. Oncol 2022, 174, 87–91. [PubMed: 34998899]
4. Vozenin M-C; Bourhis J; Durante M Towards clinical translation of FLASH radiotherapy. Nat. Rev. Clin. Oncol 2022, 19, 791–803. [PubMed: 36303024]
5. Wei S; Lin H; Choi JI; Simone CB; Kang M A Novel Proton Pencil Beam Scanning FLASH RT Delivery Method Enables Optimal OAR Sparing and Ultra-High Dose Rate Delivery: A Comprehensive Dosimetry Study for Lung Tumors. Cancers 2021, 13, 5790. [PubMed: 34830946]
6. Wei S; Lin H; Choi JI; Press RH; Lazarev S; Kabarriti R; Hajj C; Hasan S; Chhabra AM; Ii CBS; et al. FLASH Radiotherapy Using Single-Energy Proton PBS Transmission Beams for Hypofractionation Liver Cancer: Dose and Dose Rate Quantification. Front. Oncol 2022, 11, 813063. [PubMed: 35096620]
7. Mascia AE; Daugherty EC; Zhang Y; Lee E; Xiao Z; Sertorio M; Woo J; Backus LR; McDonald JM; McCann C; et al. Proton FLASH Radiotherapy for the Treatment of Symptomatic Bone Metastases: The FAST-01 Nonrandomized Trial. JAMA Oncol 2023, 9, 62–69. [PubMed: 36273324]
8. Daugherty EC; Mascia A; Zhang Y; Lee E; Xiao Z; Sertorio M; Woo J; McCann C; Russell K; Levine L; et al. FLASH Radiotherapy for the Treatment of Symptomatic Bone Metastases (FAST-01): Protocol for the First Prospective Feasibility Study. JMIR Res. Protoc 2023, 12, e41812. [PubMed: 36206189]
9. Berry RJ; Hall EJ; Forster DW; Storr TH; Goodman MJ Survival of mammalian cells exposed to X rays at ultra-high dose-rates. Br. J. Radiol 1969, 42, 102–107. [PubMed: 4975207]
10. Kim MM; Darafsheh A; Schuemann J; Dokic I; Lundh O; Zhao T; Ramos-Mendez J; Dong L; Petersson K Development of Ultra-High Dose-Rate (FLASH) Particle Therapy. IEEE Trans. Radiat. Plasma Med. Sci 2022, 6, 252–262. [PubMed: 36092270]
11. 1Esplen N; Mendonca MS; Bazalova-Carter M Physics and biology of ultrahigh dose-rate (FLASH) radiotherapy: A topical review. Phys. Med. Biol 2020, 65, 23TR03.
12. Wilson JD; Hammond EM; Higgins GS; Petersson K Ultra-High Dose Rate (FLASH) Radiotherapy: Silver Bullet or Fool’s Gold? Front. Oncol 2020, 9, 1563, Erratum in Front. Oncol. 2020, 10, 210. [PubMed: 32010633]

13. Harrington KJ Ultrahigh Dose-rate Radiotherapy: Next Steps for FLASH-RT. Clin. Cancer Res 2019, 25, 3–5. [PubMed: 30093447]
14. Montay-Gruel P; Petersson K; Jaccard M; Boivin G; Germond J-F; Petit B; Doenlen R; Favaudon V; Bochud F; Bailat C; et al. Irradiation in a flash: Unique sparing of memory in mice after whole brain irradiation with dose rates above 100 Gy/s. Radiother. Oncol 2017, 124, 365–369. [PubMed: 28545957]
15. Montay-Gruel P; Acharya MM; Gonçalves Jorge P; Petit B; Petridis IG; Fuchs P; Leavitt R; Petersson K; Gondré M; Ollivier J; et al. Hypofractionated FLASH-RT as an Effective Treatment against Glioblastoma that Reduces Neurocognitive Side Effects in Mice. Clin. Cancer Res 2021, 27, 775–784. [PubMed: 33060122]
16. Karsch L; Pawelke J; Brand M; Hans S; Hideghéty K; Jansen J; Lessmann E; Löck S; Schürer M; Schurig R; et al. Beam pulse structure and dose rate as determinants for the flash effect observed in zebrafish embryo. Radiother. Oncol 2022, 173, 49–54. [PubMed: 35661675]
17. Cecchi DD; Therriault-Proulx F; Lambert-Girard S; Hart A; Macdonald A; Pfleger M; Lenckowski M; Bazalova-Carter M Characterization of an x-ray tube-based ultrahigh dose-rate system for in vitro irradiations. Med. Phys 2021, 48, 7399–7409. [PubMed: 34528283]
18. Bazalova-Carter M; Esplen N On the capabilities of conventional x-ray tubes to deliver ultra-high (FLASH) dose rates. Med. Phys 2019, 46, 5690–5695. [PubMed: 31600830]
19. Rezaee M; Iordachita I; Wong JW Ultrahigh dose-rate (FLASH) x-ray irradiator for pre-clinical laboratory research. Phys. Med. Biol 2021, 66, 095006.
20. Gao F; Yang Y; Zhu H; Wang J; Xiao D; Zhou Z; Dai T; Zhang Y; Feng G; Li J; et al. First demonstration of the FLASH effect with ultrahigh dose rate high-energy X-rays. Radiother. Oncol 2022, 166, 44–50. [PubMed: 34774651]
21. Smyth LML; Donoghue JF; Ventura JA; Livingstone J; Bailey T; Day LRJ; Crosbie JC; Rogers PAW Comparative toxicity of synchrotron and conventional radiation therapy based on total and partial body irradiation in a murine model. Sci. Rep 2018, 8, 12044. [PubMed: 30104646]
22. Montay-Gruel P; Bouchet A; Jaccard M; Patin D; Serduc R; Aim W; Petersson K; Petit B; Bailat C; Bourhis J; et al. X-rays can trigger the FLASH effect: Ultra-high dose-rate synchrotron light source prevents normal brain injury after whole brain irradiation in mice. Radiother. Oncol 2018, 129, 582–588. [PubMed: 30177374]
23. Beyreuther E; Brand M; Hans S; Hideghéty K; Karsch L; Leßmann E; Schürer M; Szabó ER; Pawelke J Feasibility of proton FLASH effect tested by zebrafish embryo irradiation. Radiother. Oncol 2019, 139, 46–50. [PubMed: 31266652]
24. Cunningham S; McCauley S; Vairamani K; Speth J; Girdhani S; Abel E; Sharma RA; Perentesis JP; Wells SI; Mascia A; et al. FLASH Proton Pencil Beam Scanning Irradiation Minimizes Radiation-Induced Leg Contracture and Skin Toxicity in Mice. Cancers 2021, 13, 1012. [PubMed: 33804336]
25. Diffenderfer ES; Sørensen BS; Mazal A; Carlson DJ The current status of preclinical proton FLASH radiation and future directions. Med. Phys 2022, 49, 2039–2054. [PubMed: 34644403]
26. Tinganelli W; Sokol O; Quartieri M; Puspitasari A; Dokic I; Abdollahi A; Durante M; Haberer T; Debus J; Boscolo D; et al. Ultra-High Dose Rate (FLASH) Carbon Ion Irradiation: Dosimetry and First Cell Experiments. Int. J. Radiat. Oncol 2021, 112, 1012–1022.
27. Tessonnier T; Mein S; Walsh DW; Schuhmacher N; Liew H; Cee R; Galonska M; Scheloske S; Schömers C; Weber U; et al. FLASH Dose Rate Helium Ion Beams: First In Vitro Investigations. Int. J. Radiat. Oncol 2021, 111, 1011–1022.
28. Evans BT; Cooley J; Wagner MM; Yu T; Zwart T Demonstration of the FLASH Effect Within the Spread-out Bragg Peak After Abdominal Irradiation of Mice. Int. J. Part. Ther 2022, 8, 68–75. [PubMed: 35530182]
29. Darafsheh A; Hao Y; Zhao X; Zwart T; Wagner M; Evans T; Reynoso F; Zhao T Spread-out Bragg peak proton FLASH irradiation using a clinical synchrocyclotron: Proof of concept and ion chamber characterization. Med. Phys 2021, 48, 4472–4484. [PubMed: 34077590]
30. Darafsheh A; Hao Y; Zwart T; Wagner M; Catanzano D; Williamson JF; Knutson N; Sun B; Mutic S; Zhao T Feasibility of proton FLASH irradiation using a synchrocyclotron for preclinical studies. Med. Phys 2020, 47, 4348–4355. [PubMed: 32452558]

31. Hamm RW; Crandall KR; Potter JM Preliminary Design of a Dedicated Proton Therapy Linac. In Proceedings of the Conference Record of the 1991 IEEE Particle Accelerator Conference, San Francisco, CA, USA, 6–9 May 1991; Volume 4, pp. 2583–2585.
32. Lu X; Li Z; Dolgashev V; Bowden G; Sy A; Tantawi S; Nanni EA A proton beam energy modulator for rapid proton therapy. Rev. Sci. Instruments 2021, 92, 024705.
33. Degiovanni A; Amaldi U Proton and Carbon Linacs for Hadron Therapy. In Proceedings of the 27th Linear Accelerator Conference, Geneva, Switzerland, 31 August–5 September 2014; p. 6.
34. Ostroumov PN; Goel A; Mustapha B; Nassiri A; Plastun AS Compact Carbon Ion Linac. In Proceedings of the 2016 North American Particle Accelerator Conference, Chicago, IL, USA, 14 October 2016; p. 3.
35. Ungaro D; Degiovanni A; Stabile P; Sa A LIGHT: A Linear Accelerator for Proton Therapy. In Proceedings of the 2016 North American Particle Accelerator Conference, Chicago, IL, USA, 9–14 October 2016; p. 5.
36. Jolly S; Owen H; Schippers M; Welsch C Technical challenges for FLASH proton therapy. Phys. Medica Eur. J. Med. Phys 2020, 78, 71–82.
37. Benedetti S; Degiovanni A; Grudiev A; Wuensch W; Amaldi U RF design of a novel s-band backward travelling wave linac for proton therapy. In Proceedings of the 27th Linear Accelerator Conference, Geneva, Switzerland, 31 August–5 September 2014; p. 3.
38. Kutsaev SV; Agustsson R; Boucher S; Fischer R; Murokh A; Mustapha B; Nassiri A; Ostroumov PN; Plastun A; Savin E; et al. High-gradient low- β accelerating structure using the first negative spatial harmonic of the fundamental mode. Phys. Rev. Accel. Beams 2017, 20, 120401.
39. Kutsaev SV; Agustsson R; Boucher S; Chimalpopoca O; Meyer D; Murokh A; Mustapha B; Nassiri A; Smirnov AY; Smith T; et al. Test Results of a High-Gradient 2.856-GHz Negative Harmonic Accelerating Waveguide. IEEE Microw. Wirel. Components Lett 2021, 31, 1098–1101.
40. Mustapha B; Abogoda A; Barcikowski A; Fischer R; Nassiri A Design of a High-Gradient S-Band Annular Coupled Structure. In Proceedings of the 3rd North American Particle Accelerator Conference (NAPAC2019), Lansing, MI, USA, 2–6 September 2019; p. WEPLM72.
41. Matsuura T; Egashira Y; Nishio T; Matsumoto Y; Wada M; Koike S; Furusawa Y; Kohno R; Nishioka S; Kameoka S; et al. Apparent absence of a proton beam dose rate effect and possible differences in RBE between Bragg peak and plateau. Med. Phys 2010, 37, 5376–5381. [PubMed: 21089773]
42. Mustapha B; Aydogan B; Nolen J; Nassiri A; Noonan J; Pankuch M; Welsh J; Schulte R; Robb J Prospects for an advanced heavy ion therapy center in the Chicago area. AIP Conf. Proc 2019, 2160, 050009.
43. Fornek TE Advanced Photon Source Upgrade Project Preliminary Design Report; Argonne National Laboratory: Argonne, IL, USA, 2017; p. APSU-2.01-RPT-002.
44. de Walle JV; Abs M; Conjat M; Forton E; Henrotin S; Jongen Y; Kleeven W; Mandrillon J; Mandrillon P; Verbruggen P The S2C2: From Source to Extraction. In Proceedings of the Cyclotrons 2016, Zurich, Switzerland, 11–16 September 2016; p. 5.
45. Yoshimoto M; Adachi T; Aiba M; Koba K; Machida S; Mori Y; Muramatsu R; Ohmori C; Sakai I; Sato Y; et al. Recent Beam Studies of the PoP FFAG Proton Synchrotron. In Proceedings of the PACS2001. Proceedings of the 2001 Particle Accelerator Conference (Cat. No.01CH37268), Chicago, IL, USA, 18–22 June 2001; IEEE: Chicago, IL, USA, 2001; Volume 1, pp. 51–53.
46. Yonemura Y; Ikeda N; Matoba M; Aiba M; Machida S; Mori Y; Muto A; Nakano J; Ohmori C; Okabe K; et al. Development of FFAG Accelerator at KEK. In Proceedings of the 2005 Particle Accelerator Conference, Knoxville, TN, USA, 16–20 May 2005; IEEE: Knoxville, TN, USA, 2005; pp. 1943–1945.
47. Antoine S; Autin B; Beeckman W; Collot J; Conjat M; Forest F; Fourrier J; Froidefond E; Lancelot J; Mandrillon J; et al. Principle design of a protontherapy, rapid-cycling, variable energy spiral FFAG. Nucl. Instruments Methods Phys. Res. Sect. A Accel. Spectrometers, Detect. Assoc. Equip 2009, 602, 293–305.
48. Planche T; Fourrier J; Lancelot J; Méot F; Neuvéglise D; Pasternak J Design of a prototype gap shaping spiral dipole for a variable energy protontherapy FFAG. Nucl. Instruments Methods Phys. Res. Sect. A Accel. Spectrometers, Detect. Assoc. Equip 2009, 604, 435–442.

49. Available online: https://indico.fnal.gov/event/2672/contributions/77834/attachments/48652/58457/FMeot1-090921.pdf (accessed on 9 September 2022).
50. Johnstone C; Schulte R A Review of Nonscaling CW FFAs for Proton and Ion Therapy Applications; Fermi National Accelerator Lab. (FNAL): Batavia, IL USA, 2019.
51. Johnstone C; Kutsaev SV; Lanza R; Boucher S; Johnson R High-Current Light-Ion Cyclotron for Applications in Nuclear Security and Radioisotope Production. IEEE Trans. Nucl. Sci 2021, 68, 1072–1082.
52. Kutsaev SV; Johnstone C; Adonyev O; Agustsson R; Ford R; Kashikhin V Electromagnetic and Engineering Design of a High-Current 15-MeV/u Cyclotron. IEEE Trans. Nucl. Sci 2021, 68, 1083–1093.
53. Bulanov S; Esirkepov T; Khoroshkov V; Kuznetsov A; Pegoraro F Oncological hadrontherapy with laser ion accelerators. Phys. Lett. A 2002, 299, 240–247.
54. Emma C; van Tilborg J; Albert F; Labate L; England J; Gessner S; Fiuza F; Obst-Huebl L; Zholents A; Murokh A; et al. Snowmass 2021 Accelerator Frontier White Paper: Near Term Applications Driven by Advanced Accelerator Concepts. arXiv 2022, arXiv:2203.09094.
55. Strickland D; Mourou G Compression of amplified chirped optical pulses. Opt. Commun 1985, 56, 219–221.
56. Nakamura K; Mao H-S; Gonsalves AJ; Vincenti H; Mittelberger DE; Daniels J; Magana A; Toth C; Leemans WP Diagnostics, Control and Performance Parameters for the BELLA High Repetition Rate Petawatt Class Laser. IEEE J. Quantum Electron 2017, 53, 1–21.
57. Tajima T; Dawson JM Laser Electron Accelerator. Phys. Rev. Lett 1979, 43, 267–270.
58. Wilks SC; Langdon AB; Cowan TE; Roth M; Singh M; Hatchett S; Key MH; Pennington D; MacKinnon A; Snavely RA Energetic proton generation in ultra-intense laser–solid interactions. Phys. Plasmas 2001, 8, 542–549.
59. Wang X; Zgadzaj R; Fazel N; Li Z; Yi SA; Zhang X; Henderson W; Chang Y-Y; Korzekwa R; Tsai H-E; et al. Quasi-monoenergetic laser-plasma acceleration of electrons to 2 GeV. Nat. Commun 2013, 4, 1988. [PubMed: 23756359]
60. Leemans WP; Gonsalves AJ; Mao H-S; Nakamura K; Benedetti C; Schroeder CB; Tóth C; Daniels J; Mittelberger DE; Bulanov SS; et al. Multi-GeV Electron Beams from Capillary-Discharge-Guided Subpetawatt Laser Pulses in the Self-Trapping Regime. Phys. Rev. Lett 2014, 113, 245002. [PubMed: 25541775]
61. Couperus JP; Pausch R; Köhler A; Zarini O; Krämer JM; Garten M; Huebl A; Gebhardt R; Helbig U; Bock S; et al. Demonstration of a beam loaded nanocoulomb-class laser wakefield accelerator. Nat. Commun 2017, 8, 487. [PubMed: 28887456]
62. Gonsalves AJ; Nakamura K; Daniels J; Benedetti C; Pieronek C; de Raadt TCH; Steinke S; Bin JH; Bulanov SS; van Tilborg J; et al. Petawatt Laser Guiding and Electron Beam Acceleration to 8 GeV in a Laser-Heated Capillary Discharge Waveguide. Phys. Rev. Lett 2019, 122, 084801. [PubMed: 30932604]
63. Leemans WP; Geddes CGR; Faure J; Tóth C; van Tilborg J; Schroeder CB; Esarey E; Fubiani G; Auerbach D; Marcelis B; et al. Observation of Terahertz Emission from a Laser-Plasma Accelerated Electron Bunch Crossing a Plasma-Vacuum Boundary. Phys. Rev. Lett 2003, 91, 074802. [PubMed: 12935022]
64. Powers ND; Ghebregziabher I; Golovin G; Liu C; Chen S; Banerjee S; Zhang J; Umstadter D Quasi-monoenergetic and tunable X-rays from a laser-driven Compton light source. Nat. Photon 2014, 8, 28–31.
65. Phuoc KT; Corde S; Thaury C; Malka V; Tafzi A; Goddet J-P; Shah RC; Sebban S; Rousse A All-optical Compton gamma-ray source. Nat. Photon- 2012, 6, 308–311.
66. Snavely RA; Key MH; Hatchett SP; Cowan TE; Roth M; Phillips TW; Stoyer MA; Henry EA; Sangster TC; Singh MS; et al. Intense High-Energy Proton Beams from Petawatt-Laser Irradiation of Solids. Phys. Rev. Lett 2000, 85, 2945–2948. [PubMed: 11005974]
67. Hatchett SP; Brown CG; Cowan TE; Henry EA; Johnson JS; Key MH; Koch JA; Langdon AB; Lasinski BF; Lee RW; et al. Electron, photon, and ion beams from the relativistic interaction of Petawatt laser pulses with solid targets. Phys. Plasmas 2000, 7, 2076–2082.

68. Steinke S; Bin JH; Park J; Ji Q; Nakamura K; Gonsalves AJ; Bulanov SS; Thévenet M; Toth C; Vay J-L; et al. Acceleration of high charge ion beams with achromatic divergence by petawatt laser pulses. Phys. Rev. Accel. Beams 2020, 23, 021302.
69. Schreiber J; Bolton PR; Parodi K Invited Review Article: "Hands-on" laser-driven ion acceleration: A primer for laser-driven source development and potential applications. Rev. Sci. Instruments 2016, 87, 071101.
70. Macchi A; Borghesi M; Passoni M Ion acceleration by superintense laser-plasma interaction. Rev. Mod. Phys 2013, 85, 751–793.
71. Daido H; Nishiuchi M; Pirozhkov A Review of laser-driven ion sources and their applications. Rep. Prog. Phys 2012, 75, 056401. [PubMed: 22790586]
72. Higginson A; Gray RJ; King M; Dance RJ; Williamson SDR; Butler NMH; Wilson R; Capdessus R; Armstrong C; Green JS; et al. Near-100 MeV protons via a laser-driven transparency-enhanced hybrid acceleration scheme. Nat. Commun 2018, 9, 724. [PubMed: 29463872]
73. Friedl AA; Prise KM; Butterworth KT; Montay-Gruel P; Favaudon V Radiobiology of the FLASH effect. Med. Phys 2022, 49, 1993–2013. [PubMed: 34426981]
74. Bolton P; Parodi K; Schreiber J Applications of Laser-Driven Particle Acceleration; CRC Press: Boca Raton, FL, USA, 2018; ISBN 978–0-429–81709-0.
75. Durante M New challenges in high-energy particle radiobiology. Br. J. Radiol 2014, 87, 20130626. [PubMed: 24198199]
76. Kroll F; Brack F-E; Bernert C; Bock S; Bodenstein E; Brüchner K; Cowan TE; Gaus L; Gebhardt R; Helbig U; et al. Tumour irradiation in mice with a laser-accelerated proton beam. Nat. Phys 2022, 18, 316–322.
77. Yogo A; Sato K; Nishikino M; Mori M; Teshima T; Numasaki H; Murakami M; Demizu Y; Akagi S; Nagayama S; et al. Application of laser-accelerated protons to the demonstration of DNA double-strand breaks in human cancer cells. Appl. Phys. Lett 2009, 94, 181502.
78. Kraft S; Richter C; Zeil K; Bussmann M; Beyreuther E; Bock S; Bussmann M; E Cowan T; Dammene Y; Enghardt W; et al. Dose-dependent biological damage of tumour cells by laser-accelerated proton beams. New J. Phys 2010, 12, 085003.
79. Yogo A; Maeda T; Hori T; Sakaki H; Ogura K; Nishiuchi M; Sagisaka A; Kiriyama H; Okada H; Kanazawa S; et al. Measurement of relative biological effectiveness of protons in human cancer cells using a laser-driven quasimonoenergetic proton beamline. Appl. Phys. Lett 2011, 98, 053701.
80. Bin J; Allinger K; Assmann W; Dollinger G; Drexler GA; Friedl AA; Habs D; Hilz P; Hoerlein R; Humble N; et al. A laser-driven nanosecond proton source for radiobiological studies. Appl. Phys. Lett 2012, 101, 243701.
81. Doria D; Kakolee KF; Kar S; Litt SK; Fiorini F; Ahmed H; Green S; Jeynes JCG; Kavanagh J; Kirby D; et al. Biological effectiveness on live cells of laser driven protons at dose rates exceeding 10^9Gy/s. AIP Adv 2012, 2, 011209.
82. Raschke S; Spickermann S; Toncian T; Swantusch M; Boeker J; Giesen U; Iliakis G; Willi O; Boege F Ultra-short laser-accelerated proton pulses have similar DNA-damaging effectiveness but produce less immediate nitroxidative stress than conventional proton beams. Sci. Rep 2016, 6, 32441. [PubMed: 27578260]
83. Manti L; Perozziello F; Borghesi M; Candiano G; Chaudhary P; Cirrone G; Doria D; Gwynne D; Leanza R; Prise KM; et al. The radiobiology of laser-driven particle beams: Focus on sub-lethal responses of normal human cells. J. Instrum 2017, 12, C03084.
84. Bayart E; Flacco A; Delmas O; Pommarel L; Levy D; Cavallone M; Megnin-Chanet F; Deutsch E; Malka V Fast dose fractionation using ultra-short laser accelerated proton pulses can increase cancer cell mortality, which relies on functional PARP1 protein. Sci. Rep 2019, 9, 10132. [PubMed: 31300704]
85. Hanton F; Chaudhary P; Doria D; Gwynne D; Maiorino C; Scullion C; Ahmed H; Marshall T; Naughton K; Romagnani L; et al. DNA DSB Repair Dynamics following Irradiation with Laser-Driven Protons at Ultra-High Dose Rates. Sci. Rep 2019, 9, 1–10. [PubMed: 30626917]
86. Rösch TF; Szabó Z; Haffa D; Bin J; Brunner S; Englbrecht FS; Friedl AA; Gao Y; Hartmann J; Hilz P; et al. A feasibility study of zebrafish embryo irradiation with laser-accelerated protons. Rev. Sci. Instruments 2020, 91, 063303.

87. Han J; Mei Z; Lu C; Qian J; Liang Y; Sun X; Pan Z; Kong D; Xu S; Liu Z; et al. Ultra-High Dose Rate FLASH Irradiation Induced Radio-Resistance of Normal Fibroblast Cells Can Be Enhanced by Hypoxia and Mitochondrial Dysfunction Resulting From Loss of Cytochrome C. Front. Cell Dev. Biol 2021, 9, 672929. [PubMed: 33996831]

88. Bin J; Obst-Huebl L; Mao J-H; Nakamura K; Geulig LD; Chang H; Ji Q; He L; De Chant J; Kober Z; et al. A new platform for ultra-high dose rate radiobiological research using the BELLA PW laser proton beamline. Sci. Rep 2022, 12, 1484. [PubMed: 35087083]

89. Laschinsky L; Baumann M; Beyreuther E; Enghardt W; Kaluza M; Karsch L; Lessmann E; Naumburger D; Nicolai M; Richter C; et al. Radiobiological effectiveness of laser accelerated electrons in comparison to electron beams from a conventional linear accelerator. J. Radiat. Res 2012, 53, 395–403. [PubMed: 22739009]

90. Labate L; Andreassi MG; Baffigi F; Basta G; Bizzarri R; Borghini A; Candiano GC; Casarino C; Cresci M; Di Martino F; et al. Small-scale laser based electron accelerators for biology and medicine: A comparative study of the biological effectiveness. 2013, 8779, 87790O. Proceedings 2013, 8779, 87790O.

91. Oppelt M; Baumann M; Bergmann R; Beyreuther E; Brüchner K; Hartmann J; Karsch L; Krause M; Laschinsky L; Leßmann E; et al. Comparison study of in vivo dose response to laser-driven versus conventional electron beam. Radiat. Environ. Biophys 2015, 54, 155–166. [PubMed: 25600561]

92. Andreassi MG; Borghini A; Pulignani S; Baffigi F; Fulgentini L; Koester P; Cresci M; Vecoli C; Lamia D; Russo G; et al. Radiobiological Effectiveness of Ultrashort Laser-Driven Electron Bunches: Micronucleus Frequency, Telomere Shortening and Cell Viability. Radiat. Res 2016, 186, 245–253. [PubMed: 27439449]

93. Babayan N; Grigoryan B; Khondkaryan L; Tadevosyan G; Sarkisyan N; Grigoryan R; Apresyan L; Aroutiounian R; Vorobyeva N; Pustovalova M; et al. Laser-Driven Ultrashort Pulsed Electron Beam Radiation at Doses of 0.5 and 1.0 Gy Induces Apoptosis in Human Fibroblasts. Int. J. Mol. Sci 2019, 20, 5140. [PubMed: 31627284]

94. Cavallone M; Rovige L; Huijts J; Bayart É; Delorme R; Vernier A; Gonçalves Jorge P; Moeckli R; Deutsch E; Faure J; et al. Dosimetric characterisation and application to radiation biology of a kHz laser-driven electron beam. Appl. Phys. B 2021, 127, 57.

95. Desrosiers C; Moskvin V; Bielajew AF; Papiez L 150–250 MeV electron beams in radiation therapy. Phys. Med. Biol 2000, 45, 1781–1805. [PubMed: 10943919]

96. Kokurewicz K; Welsh GH; Brunetti E; Wiggins SM; Boyd M; Sorensen A; Chalmers A; Schettino G; Subiel A; DesRosiers C; et al. Laser-Plasma Generated Very High Energy Electrons (VHEEs) in Radiotherapy; SPIE: Bellingham, WA, USA, 2017.

97. Labate L; Palla D; Panetta D; Avella F; Baffigi F; Brandi F; Di Martino F; Fulgentini L; Giulietti A; Köster P; et al. Toward an effective use of laser-driven very high energy electrons for radiotherapy: Feasibility assessment of multi-field and intensity modulation irradiation schemes. Sci. Rep 2020, 10, 17307. [PubMed: 33057078]

98. Svendsen K; Guénot D; Svensson JB; Petersson K; Persson A; Lundh O A focused very high energy electron beam for fractionated stereotactic radiotherapy. Sci. Rep 2021, 11, 5844. [PubMed: 33712653]

99. Pommarel L; Vauzour B; Mégnin-Chanet F; Bayart E; Delmas O; Goudjil F; Nauraye C; Letellier V; Pouzoulet F; Schillaci F; et al. Spectral and spatial shaping of a laser-produced ion beam for radiation-biology experiments. Phys. Rev. Accel. Beams 2017, 20, 032801.

100. Brack F-E; Kroll F; Gaus L; Bernert C; Beyreuther E; Cowan TE; Karsch L; Kraft S; Kunz-Schughart LA; Lessmann E; et al. Spectral and spatial shaping of laser-driven proton beams using a pulsed high-field magnet beamline. Sci. Rep 2020, 10, 9118. [PubMed: 32499539]

101. Cirrone GAP; Petringa G; Catalano R; Schillaci F; Allegra L; Amato A; Avolio R; Costa M; Cuttone G; Fajstavr A; et al. ELIMED-ELIMAIA: The First Open User Irradiation Beamline for Laser-Plasma-Accelerated Ion Beams. Front. Phys 2020, 8, 437.

102. Brüchner K; Beyreuther E; Baumann M; Krause M; Oppelt M; Pawelke J Establishment of a small animal tumour model for in vivo studies with low energy laser accelerated particles. Radiat. Oncol 2014, 9, 57. [PubMed: 24533586]

103. van Tilborg J; Steinke S; Geddes CGR; Matlis NH; Shaw BH; Gonsalves AJ; Huijts JV; Nakamura K; Daniels J; Schroeder CB; et al. Active Plasma Lensing for Relativistic Laser-Plasma-Accelerated Electron Beams. Phys. Rev. Lett 2015, 115, 184802. [PubMed: 26565471]
104. Linz U; Alonso J Laser-driven ion accelerators for tumor therapy revisited. Phys. Rev. Accel. Beams 2016, 19, 124802.
105. Masood U; Cowan TE; Enghardt W; Hofmann KM; Karsch L; Kroll F; Schramm U; Wilkens JJ; Pawelke J A light-weight compact proton gantry design with a novel dose delivery system for broad-energetic laser-accelerated beams. Phys. Med. Biol 2017, 62, 5531–5555. [PubMed: 28609301]
106. Hofmann KM; Masood U; Pawelke J; Wilkens JJ A treatment planning study to assess the feasibility of laser-driven proton therapy using a compact gantry design. Med. Phys 2015, 42, 5120–5129. [PubMed: 26328963]
107. Gotz M; Karsch L; Pawelke J A new model for volume recombination in plane-parallel chambers in pulsed fields of high dose-per-pulse. Phys. Med. Biol 2017, 62, 8634–8654. [PubMed: 28858855]
108. Geulig LD; Obst-Huebl L; Nakamura K; Bin J; Ji Q; Steinke S; Snijders AM; Mao J-H; Blakely EA; Gonsalves AJ; et al. Online charge measurement for petawatt laser-driven ion acceleration. Rev. Sci. Instruments 2022, 93, 103301.
109. Bin JH; Ji Q; Seidl PA; Raftrey D; Steinke S; Persaud A; Nakamura K; Gonsalves A; Leemans WP; Schenkel T Absolute calibration of GafChromic film for very high flux laser driven ion beams. Rev. Sci. Instruments 2019, 90, 053301.
110. Richter C; Karsch L; Dammene Y; Kraft S; Metzkes-Ng J; Schramm U; Schürer M; Sobiella M; Weber A; Zeil K; et al. A dosimetric system for quantitative cell irradiation experiments with laser-accelerated protons. Phys. Med. Biol 2011, 56, 1529–1543. [PubMed: 21325708]
111. Zeil K; Baumann M; Beyreuther E; Burris-Mog T; Cowan TE; Enghardt W; Karsch L; Kraft S; Laschinsky L; Metzkes-Ng J; et al. Dose-controlled irradiation of cancer cells with laser-accelerated proton pulses. Appl. Phys. B 2013, 110, 437–444.
112. Esirkepov T; Borghesi M; Bulanov SV; Mourou G; Tajima T Highly Efficient Relativistic-Ion Generation in the Laser-Piston Regime. Phys. Rev. Lett 2004, 92, 175003. [PubMed: 15169160]
113. Park J; Bulanov SS; Bin J; Ji Q; Steinke S; Vay J-L; Geddes CGR; Schroeder C; Leemans WP; Schenkel T; et al. Ion acceleration in laser generated megatesla magnetic vortex. Phys. Plasmas 2019, 26, 103108.
114. Fiuza F; Stockem A; Boella E; Fonseca RA; Silva LO; Haberberger D; Tochitsky S; Mori WB; Joshi C Ion acceleration from laser-driven electrostatic shocks. Phys. Plasmas 2013, 20, 056304.
115. Kiani L; Zhou T; Bahk S-W; Bromage J; Bruhwiler D; Campbell EM; Chang Z; Chowdhury E; Downer M; Du Q; et al. High Average Power Ultrafast Laser Technologies for Driving Future Advanced Accelerators. arXiv 2022, arXiv:2204.10774.
116. Vozenin M; Herman D Suit Plenary Lecture - From Irradiation at Ultrahigh Dose Rate to FLASH Radiotherapy: New Radiobiology to Support Clinical Translation. arXiv 2022, arXiv:2204.10774. Presented at the 67th Annual International Research Society.
117. Acharya S; Bhat NN; Joseph P; Sanjeev G; Sreedevi B; Narayana Y Dose rate effect on micronuclei induction in human blood lymphocytes exposed to single pulse and multiple pulses of electrons. Radiat. Environ. Biophys 2011, 50, 253–263. [PubMed: 21259020]
118. Takayama K; Briggs RJ (Eds.). Induction Accelerators; Springer: Heidelberg, Germany; New York, NY, USA, 2010; ISBN 978–3-642–13916-1.
119. Barnard JJ; Bangerter RO; Faltens A; Fessenden TJ; Friedman A; Lee EP; Logan BG; Lund SM; Meier W; Sharp WM; et al. Induction Accelerator Architectures for Heavy-Ion Fusion1Work Performed under the Auspices of the US Department of Energy at LLNL under Contract W-7405-ENG-48 and at LBNL by the Director, Office of Energy Research, Advanced Energy Projects Division, US D.O.E. under Contract DE-AC03–76SF00098.1. Nucl. Instrum. Methods Phys. Res. Sect. A Accel. Spectrometers Detect. Assoc. Equip 1998, 415, 218–228.
120. Smith JR; Bailey VL; Lackner H; Putnam SD Performance of the Spiral Line Induction Accelerator; IEEE: New York, NY, USA, 1997.

121. Sampayan SE; Sampayan KC; Caporaso GJ; Chen Y-J; Falabella S; Hawkins SA; Hearn J; Watson JA; Zentler J-M Megavolt bremsstrahlung measurements from linear induction accelerators demonstrate possible use as a FLASH radiotherapy source to reduce acute toxicity. Sci. Rep 2021, 11, 17104. [PubMed: 34429440]

122. Panofsky WKH; Bander M Asymptotic Theory of Beam Break-Up in Linear Accelerators. Rev. Sci. Instruments 1968, 39, 206–212.

123. Stanley H Jr. Charged Particle Beams; Reprinted; Dover Publications: New York, NY, USA, 2013; ISBN 978–0-486–49868-3.

124. Uetomi I; Yamazaki M; Kobayashi H; Sato I Extended Theory of Beam Loading in Electron Linac. Jpn. J. Appl. Phys 1993, 32, 2858–2864.

125. Multhauf LG; Back NL; Simmons LF; Zentler J-M; Scarpetti RD The LLNL flash X-ray induction linear accelerator (FXR). Proceedings 2003, 4948, 622–633.

126. Nexsen WE; Atkinson DP; Barrett DM; Chen Y-J; Clark JC; Griffith LV; Kirbie HC; Newton MA; Paul AC; Sampayan S; et al. The ETA-II induction linac as a high-average-power FEL driver. Nucl. Instruments Methods Phys. Res. Sect. A Accel. Spectrometers, Detect. Assoc. Equip 1990, 296, 54–61.

127. Negre JP; Rubbelynck C Application of fast CVD diamond photoconductor detectors to MeV X-ray metrology for the AIRIX flash radiographic facility. Nucl. Instruments Methods Phys. Res. Sect. A Accel. Spectrometers, Detect. Assoc. Equip 2000, 451, 638–650.

128. Thumm M State-of-the-Art of High-Power Gyro-Devices and Free Electron Masers. J. Infrared Millim. Terahertz Waves 2020, 41, 1–140.

129. Fryar CD; Kruszon-Moran D; Gu Q; Ogden CL Mean Body Weight, Height, Waist Circumference, and Body Mass Index Among Adults: United States, 1999–2000 Through 2015–2016. Natl. Health Stat. Rep 2018, 1–16.

130. Durante M; Paganetti H Nuclear physics in particle therapy: A review. Rep. Prog. Phys 2016, 79, 096702. [PubMed: 27540827]

131. Svensson R; Brahme A Effective source size, yield and beam profile from multi-layered bremsstrahlung targets. Phys. Med. Biol 1996, 41, 1353–1379. [PubMed: 8858725]

132. Kutsaev SV Advanced Technologies for Applied Particle Accelerators and Examples of Their Use (Review). Tech. Phys 2021, 66, 161–195.

133. Kutsaev S; Agustsson R; Arodzero A; Berry R; Bezhanov A; Boucher S; Chimalpopoca O; Diego A; Faillace L; Gavryushkin D; et al. Compact X-Band electron linac for radiotherapy and security applications. Radiat. Phys. Chem 2021, 185, 109494.

134. Kutsaev SV; Agustsson R; Arodzero A; Berry R; Boucher S; Diego A; Gavryushkin D; Hartzell JJ; Lanza RC; Smirnov AY; et al. Linear accelerator for security, industrial and medical applications with rapid beam parameter variation. Radiat. Phys. Chem 2021, 183, 109398.

135. Boucher S; Agustsson R; Kutsaev S Linear Accelerator for Generating High X-ray Doses. U.S. Patent WO2021113323A1, 6 October 2021.

136. Lyu Q; Neph R; O'connor D; Ruan D; Boucher S; Sheng K ROAD: ROtational direct Aperture optimization with a Decoupled ring-collimator for FLASH radiotherapy. Phys. Med. Biol 2021, 66, 035020. [PubMed: 33207321]

137. Lempart M; Blad B; Adrian G; Bäck S; Knöös T; Ceberg C; Petersson K Modifying a clinical linear accelerator for delivery of ultra-high dose rate irradiation. Radiother. Oncol 2019, 139, 40–45. [PubMed: 30755324]

138. Kutsaev SV Electron bunchers for industrial RF linear accelerators: Theory and design guide. Eur. Phys. J. Plus 2021, 136, 446.

139. Kutsaev S; Agustsson R; Boucher S; Kaneta K; Smirnov AY; Yu V Linear accelerator for demonstration of X-ray radiotherapy with flash effect. In LINAC; JACoW Publishing: Liverpool, UK, 2022.

140. Gao H; Lin B; Lin Y; Fu S; Langen K; Liu T; Bradley J Simultaneous dose and dose rate optimization (SDDRO) for FLASH proton therapy. Med. Phys 2020, 47, 6388–6395. [PubMed: 33068294]

141. Maxim PG; Tantawi SG; Loo BW PHASER: A platform for clinical translation of FLASH cancer radiotherapy. Radiother. Oncol 2019, 139, 28–33. [PubMed: 31178058]

142. Tantawi S; Nasr M; Li Z; Limborg C; Borchard P Design and demonstration of a distributed-coupling linear accelerator structure. Phys. Rev. Accel. Beams 2020, 23, 092001.

143. Nasr M; Nanni E; Breidenbach M; Weathersby S; Oriunno M; Tantawi S Experimental demonstration of particle acceleration with normal conducting accelerating structure at cryogenic temperature. Phys. Rev. Accel. Beams 2021, 24, 093201.

144. Simmons DA; Lartey FM; Schüler E; Rafat M; King G; Kim A; Ko R; Semaan S; Gonzalez S; Jenkins M; et al. Reduced cognitive deficits after FLASH irradiation of whole mouse brain are associated with less hippocampal dendritic spine loss and neuroinflammation. Radiother. Oncol 2019, 139, 4–10. [PubMed: 31253467]

145. Schüler E; Trovati S; King G; Lartey F; Rafat M; Villegas M; Praxel AJ; Loo BW; Maxim PG Experimental Platform for Ultra-high Dose Rate FLASH Irradiation of Small Animals Using a Clinical Linear Accelerator. Int. J. Radiat. Oncol. Biol. Phys 2017, 97, 195–203. [PubMed: 27816362]

146. Lagzda A; Aitkenhead A; Corsini R; Farabolini W; Jones R; Kirkby K; MacKay R; Van Herk M Very-High Energy Electron (VHEE) Studies at CERN's CLEAR User Facility. In Proceedings of the 9th International Particle Accelerator Conference, Vancouver, Canada, 29 April–4 May 2018.

147. Rahman M; Ashraf MR; Zhang R; Bruza P; Dexter CA; Thompson L; Cao X; Williams BB; Hoopes PJ; Pogue BW; et al. Electron FLASH Delivery at Treatment Room Isocenter for Efficient Reversible Conversion of a Clinical LINAC. Int. J. Radiat. Oncol. Biol. Phys 2021, 110, 872–882. [PubMed: 33444695]

148. Jaccard M; Durán MT; Petersson K; Germond J-F; Liger P; Vozenin M-C; Bourhis J; Bochud F; Bailat C High dose-perpulse electron beam dosimetry: Commissioning of the Oriatron eRT6 prototype linear accelerator for preclinical use. Med. Phys 2018, 45, 863–874. [PubMed: 29206287]

149. Lansonneur P; Favaudon V; Heinrich S; Fouillade C; Verrelle P; De Marzi L Simulation and experimental validation of a prototype electron beam linear accelerator for preclinical studies. Phys. Med 2019, 60, 50–57. [PubMed: 31000086]

150. Felici G; Barca P; Barone S; Bortoli E; Borgheresi R; De Stefano S; Di Francesco M; Grasso L; Linsalata S; Marfisi D; et al. Transforming an IORT Linac Into a FLASH Research Machine: Procedure and Dosimetric Characterization. Front. Phys 2020, 8.

151. Moeckli R; Gonçalves Jorge P; Grilj V; Oesterle R; Cherbuin N; Bourhis J; Vozenin MC; Germond JF; Bochud F; Bailat C Commissioning of an ultra-high dose rate pulsed electron beam medical LINAC for FLASH RT preclinical animal experiments and future clinical human protocols. Med. Phys 2021, 48, 3134–3142. [PubMed: 33866565]

152. PMB-Alcen Announces the Launch of FLASHKNiFE, the FLASH Radiotherapy System Dedicated to Clinical Trials. Available online: https://www.pmb-alcen.com/en/news/pmb-alcen-announces-launch-flashknife-flash-radiotherapy-system-dedicatedclinical-trials (accessed on 9 September 2022).

153. NOVAC 11—Soiort. Available online: https://www.soiort.com/novac-11/ (accessed on 9 September 2022).

154. Palma B; Bazalova-Carter M; Hårdemark B; Hynning E; Qu B; Loo BW; Maxim PG Assessment of the quality of very high-energy electron radiotherapy planning. Radiother. Oncol 2016, 119, 154–158. [PubMed: 26898508]

155. Schüler E; Eriksson K; Hynning E; Hancock SL; Hiniker SM; Bazalova-Carter M; Wong T; Le Q-T; Loo BW Jr.; Maxim PG Very high-energy electron (VHEE) beams in radiation therapy—Treatment plan comparison between VHEE, VMAT, and PPBS. Med. Phys 2017, 44, 2544–2555. [PubMed: 28339108]

156. Papiez L; Desrosiers C; Moskvin V Very High Energy Electrons (50–250 MeV) and Radiation Therapy. Technol. Cancer Res. Treat 2002, 1, 105–110. [PubMed: 12622516]

157. Bazalova-Carter M; Qu B; Palma B; Hårdemark B; Hynning E; Jensen C; Maxim PG; Loo BW Treatment planning for radiotherapy with very high-energy electron beams and comparison of VHEE and VMAT plans. Med. Phys 2015, 42, 2615–2625. [PubMed: 25979053]

158. Wuensch W The CHUV-CERN Facility for FLASH Treatment of Large, Deep-Seated Tumors: The DEFT (Deep Electron FLASH Therapy) Facility. In Proceedings of the FLASH Radiotherapy & Particle Therapy Conference, Barcelona, Spain, 1–3 December 2021.

159. Han Y; Golfe AF; Vallerand C; Bai B; Duchesne P; Prezado Y; Delorme R; Poortmans P; Favaudon V; Fouillade C; et al. Optics Design and Beam Dynamics simulation for a VHEE Radiobiology beam line at PRAE accelerator. J. Phys. Conf. Ser 2019, 1350, 012200.

160. Farkas ZD; Hoag HA; Loew GA; Wilson PB SLED: A Method of Doubling SLAC's Energy. In Proceedings of the 9th International Conference on High-Energy Accelerators, Stanford, CA, USA, 2–7 May 1974; pp. 576–583.

161. Wilson PB; Farkas ZD; Ruth RD SLED-II: A New Method of RF Pulse Compression. In Proceedings of the 15th International Linear Accelerator Conference, Albuquerque, NM, USA, 9–14 September 1990.

162. Farkas Z Binary Peak Power Multiplier and its Application to Linear Accelerator Design. IEEE Trans. Microw. Theory Tech 1986, 34, 1036–1043.

163. Wang JW; Tantawi SG; Xu C; Franzi M; Krejcik P; Bowden G; Condamoor S; Ding Y; Dolgashev V; Eichner J; et al. Development for a supercompact X -band pulse compression system and its application at SLAC. Phys. Rev. Accel. Beams 2017, 20, 110401.

164. Franzi M; Wang J; Dolgashev V; Tantawi S Compact rf polarizer and its application to pulse compression systems. Phys. Rev. Accel. Beams 2016, 19, 062002.

165. Bai M; Barklow T; Bartoldus R; Breidenbach M; Grenier P; Huang Z; Kagan M; Lewellen J; Li Z; Markiewicz TW; et al. C$ˆ3$: A "Cool" Route to the Higgs Boson and Beyond. arXiv 2021, arXiv:2110.15800.

166. Nanni EA; Breidenbach M; Vernieri C; Belomestnykh S; Bhat P; Nagaitsev S; Bai M; Berg W; Barklow T; Byrd J; et al. C$ˆ3$ Demonstration Research and Development Plan. arXiv 2022, arXiv:2203.09076.

167. Martínez-Rovira I; Fois G; Prezado Y Dosimetric evaluation of new approaches in GRID therapy using nonconventional radiation sources. Med. Phys 2015, 42, 685–693. [PubMed: 25652482]

168. Snively E; Deering K; Nanni E mm-Wave Linac Design for Next Generation VHEE Cancer Therapy Systems. In Proceedings of the 12th International Particle Accelerator Conference, Online, 24–28 May 2021.

169. Nanni EA; Dolgashev VA; Haase A; Neilson J; Tantawi S; Schaub SC; Temkin R; Spataro B Prototyping high-gradient mm-wave accelerating structures. J. Phys. Conf. Ser 2017, 874, 012039.

170. Othman M Others Initial Results of High-Gradient Breakdown Tests for W-Band Accelerating Structures. In Proceedings of the 10th International Particle Accelerator Conference, Melbourne, Australia, 19–24 May 2019; p. THPGW080.

171. Snively E; Othman M; Deering K; Kuppusamy S; Wehner G High Gradient Mm-Wave Linac for VHEE Therapy. In Proceedings of the FLASH Radiotherapy & Particle Therapy Conference, Barcelona, Spain, 12 May 2021.

172. Kutsaev SV; Jacobson B; Smirnov AY; Campese T; Dolgashev VA; Goncharik V; Harrison M; Murokh A; Nanni E; Picard J; et al. Nanosecond rf-Power Switch for Gyrotron-Driven Millimeter-Wave Accelerators. Phys. Rev. Appl 2019, 11, 034052.

173. Othman MAK; Picard J; Schaub S; Dolgashev VA; Lewis SM; Neilson J; Haase A; Jawla S; Spataro B; Temkin RJ; et al. Experimental demonstration of externally driven millimeter-wave particle accelerator structure. Appl. Phys. Lett 2020, 117, 073502.

174. Lewis S; Dolgashev V; Haase A; Kim D; Nanni E; Othman M; Simakov E; Sy A; Tantawi S Design of a High Gradient THz-Driven Electron Gun. In Proceedings of the 10th International Particle Accelerator Conference, Melbourne, Australia, 19–24 May 2019; p. TUPTS077.

175. Holger G Dose Delivery System of the Varian ProBeam System with Continuous Beam. In Proceedings of the Workshop on Innovative Delivery Systems in Particle Therapy, Torino, Italy, 24 February 2017.

176. Pedroni E; Bacher R; Blattmann H; Böhringer T; Coray A; Lomax A; Lin S; Munkel G; Scheib S; Schneider U The 200-MeV proton therapy project at the Paul Scherrer Institute: Conceptual design and practical realization. Med. Phys 1995, 22, 37–53. [PubMed: 7715569]

177. FlashForward Consortium | Varian. Available online: https://www.varian.com/about-varian/research/flashforwardconsortium (accessed on 18 November 2022).

178. Calaga R; De Maria R; Barranco J; Giovannozzi M; Grudiev A; Tomas R Study of Multipolar RF Kicks from the Main Deflecting Mode in Compact Crab Cavities for LHC. Conf. Proc. C 2012, 1205201, 1873–1875.

179. Snively E Deflector Cavity Design for Rapid 2-D Proton Beam Scanning. In Proceedings of the APS March Meeting, Denver, CO, USA, 2–6 March 2020.

180. Dasu S; Nanni EA; Peskin ME; Vernieri C; Barklow T; Bartoldus R; Bhat PC; Black K; Brau J; Breidenbach M; et al. Strategy for Understanding the Higgs Physics: The Cool Copper Collider. arXiv 2022, arXiv:2203.07646.

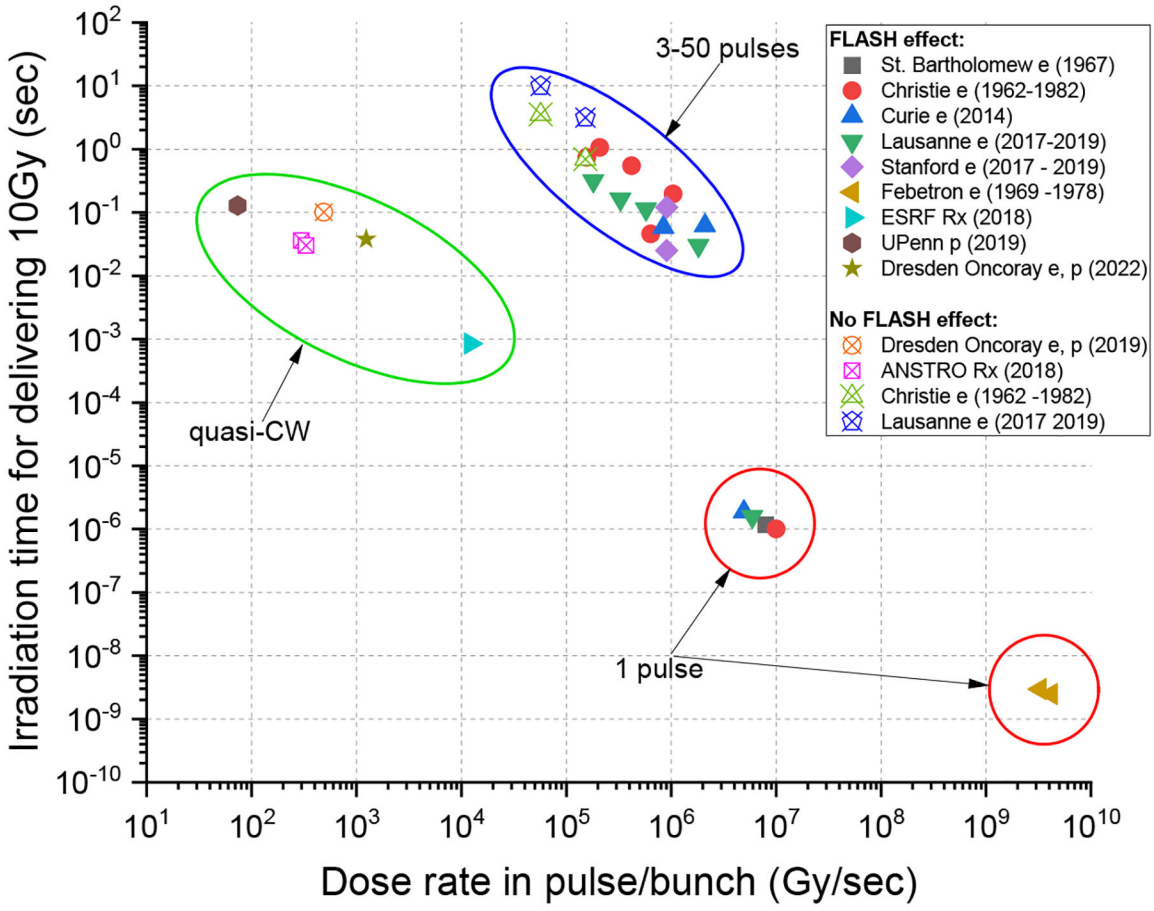

Figure 1.

Summary of preclinical studies at different accelerator facilities with different radiation types (right panel). Note the irradiation time for delivering 10 Gy on the vertical axis and the IDR of linac pulses or CW bunches on the horizontal axis. The FLASH effect has been observed for a wide IDR range of repeated linac pulses and different types of quasi-CW bunch delivery with iso-cyclotrons and synchrotron radiation light sources. FLASH effects were also seen with single electron pulses with IDR in the range of 10^6–10^7 Gy/s and 10^9–10^{10} Gy/s, respectively. Modified from Montay-Gruel P et al. [15]; for references of the individual data points, see that publication. We added the data point from Karsch et al. [16] and grouped the data according to delivery method.

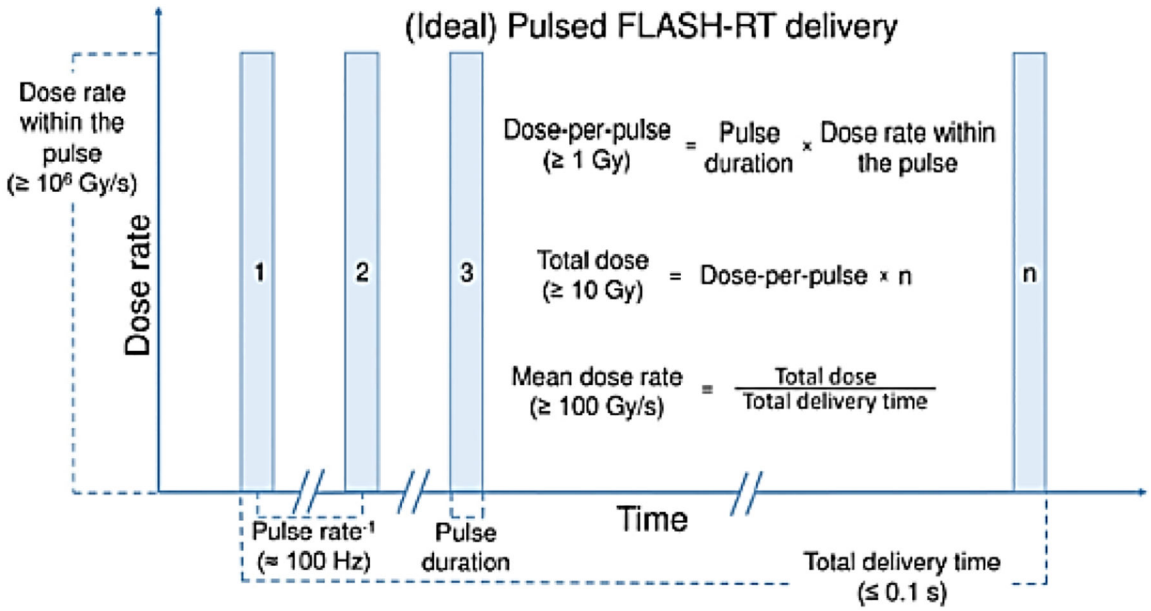

Figure 2.

Schematic view of pulsed beam delivery inducing the FLASH effect. (Reproduced from Wilson et al. [12] under the terms of the Creative Commons Attribution License (CC BY), http://creativecommons.org/licenses/by/4.0/) (accessed on 9 September 2022).

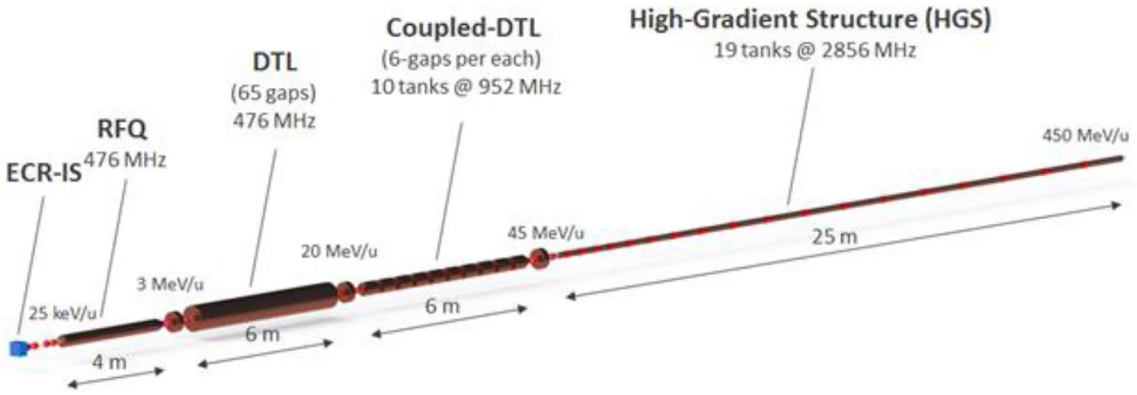

Figure 3.
Layout of the proposed ACCIL design.

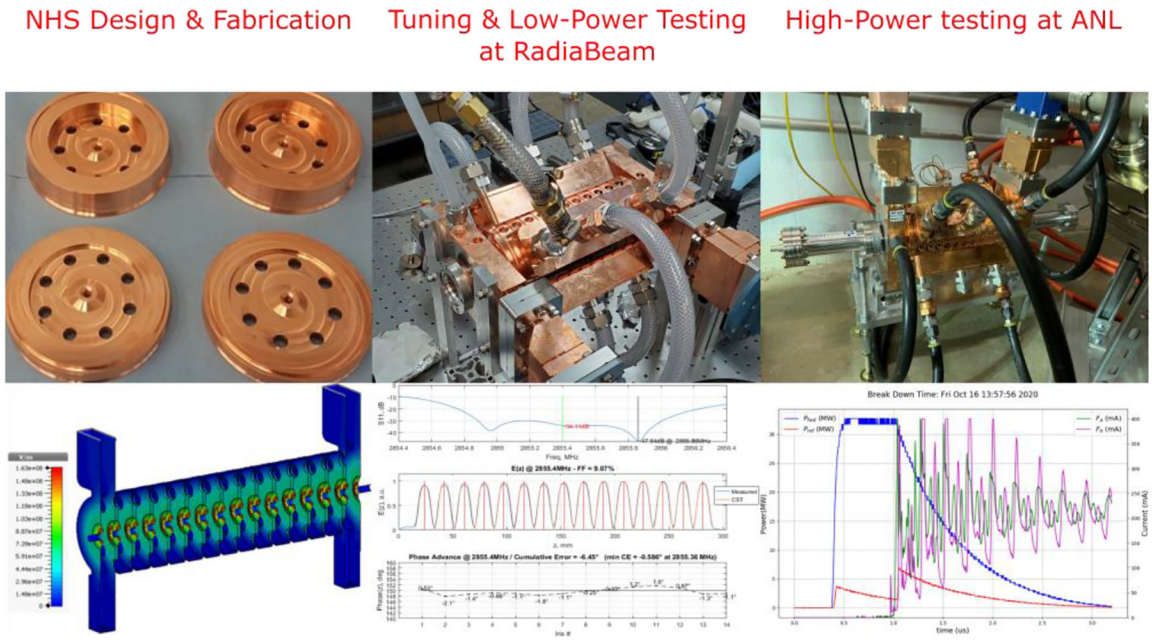

Figure 4.

Design, fabrication, and high-power testing of the negative-harmonic traveling-wave structure (NHS) developed by RadiaBeam in collaboration with Argonne.

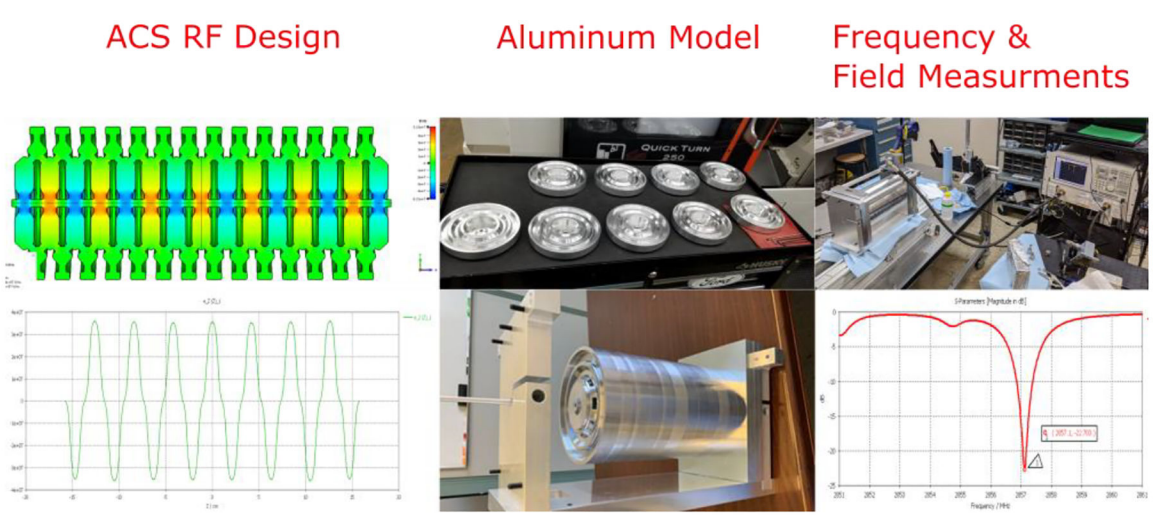

Figure 5.
Design, cold model, and measurements of the annular-coupled structure (ACS) developed by Argonne in collaboration with RadiaBeam.

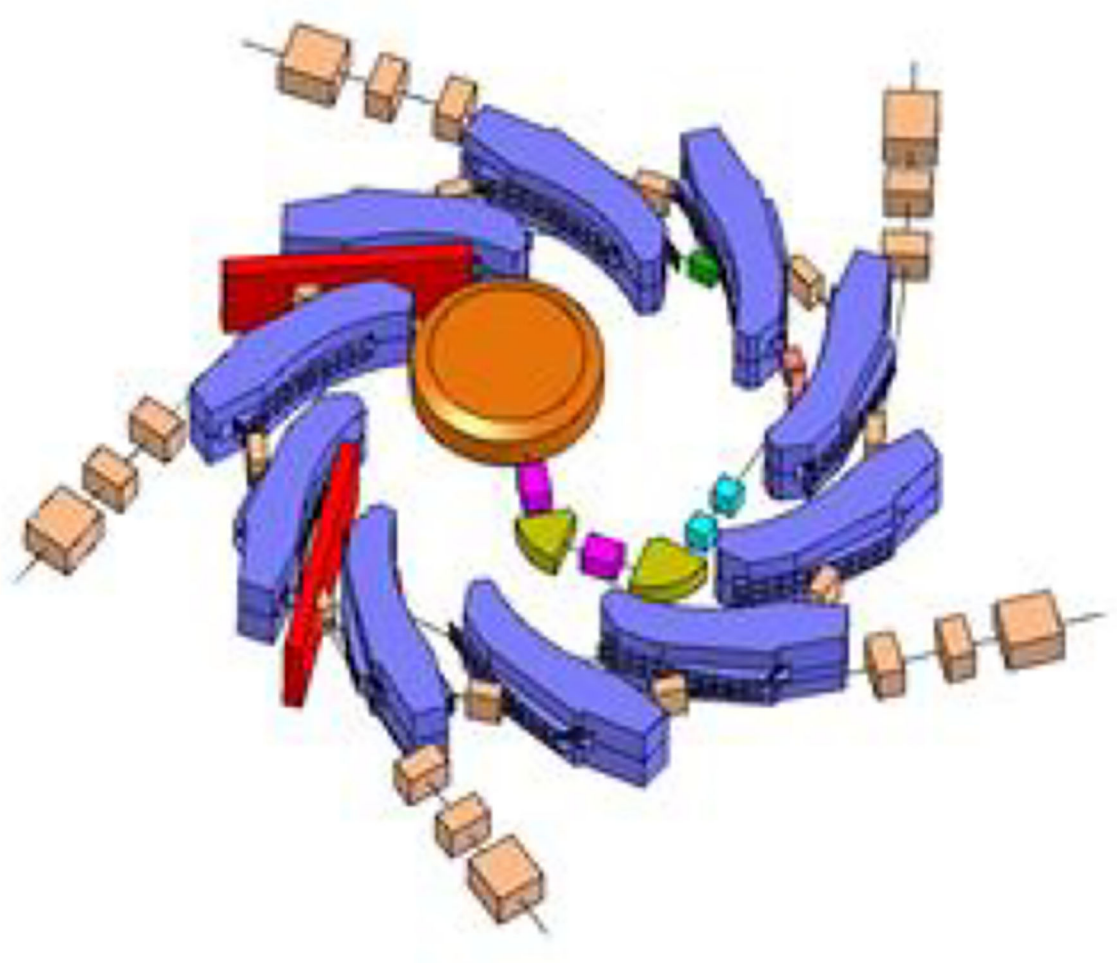

Figure 6.
RACCAM multiple-extraction proton therapy FFGA ring. Reproduced with permission from Ref. [49].

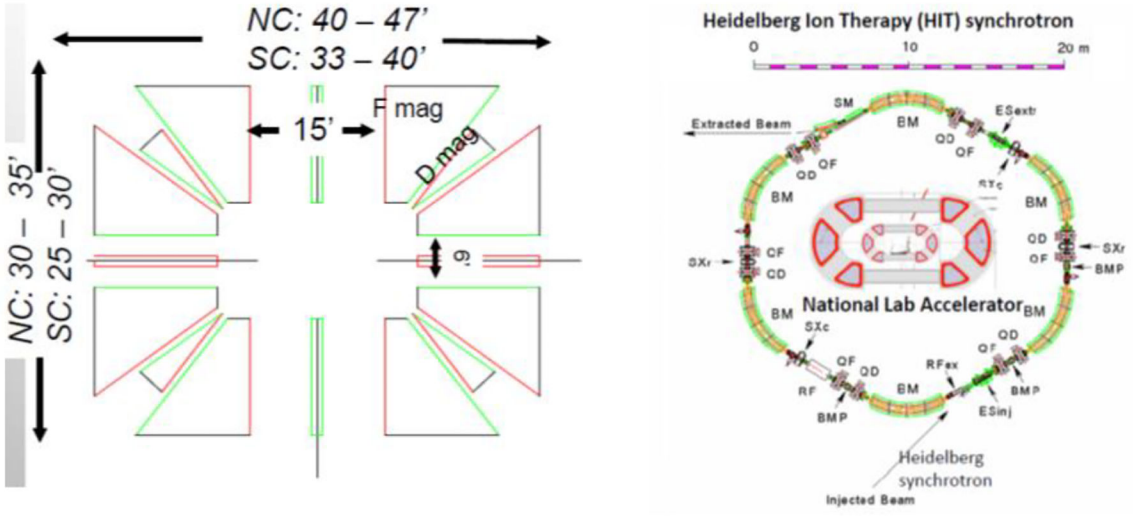

Figure 7.

Outer dimensions for a variable energy 330 MeV/nucleon therapeutic ring (**left**) and a dual ring system of 430 MeV/nucleon (**right**) compared with the Heidelberg ion therapy facility. On the right, the FLASH-capable, CW, and variable-energy 430-MeV/nucleon ion accelerator nested system is compared to equivalent-energy, low-duty-cycle Heidelberg ion therapy synchrotron. Inner ring racetrack is 250 MeV/nucleon and can provide independent beam delivery.

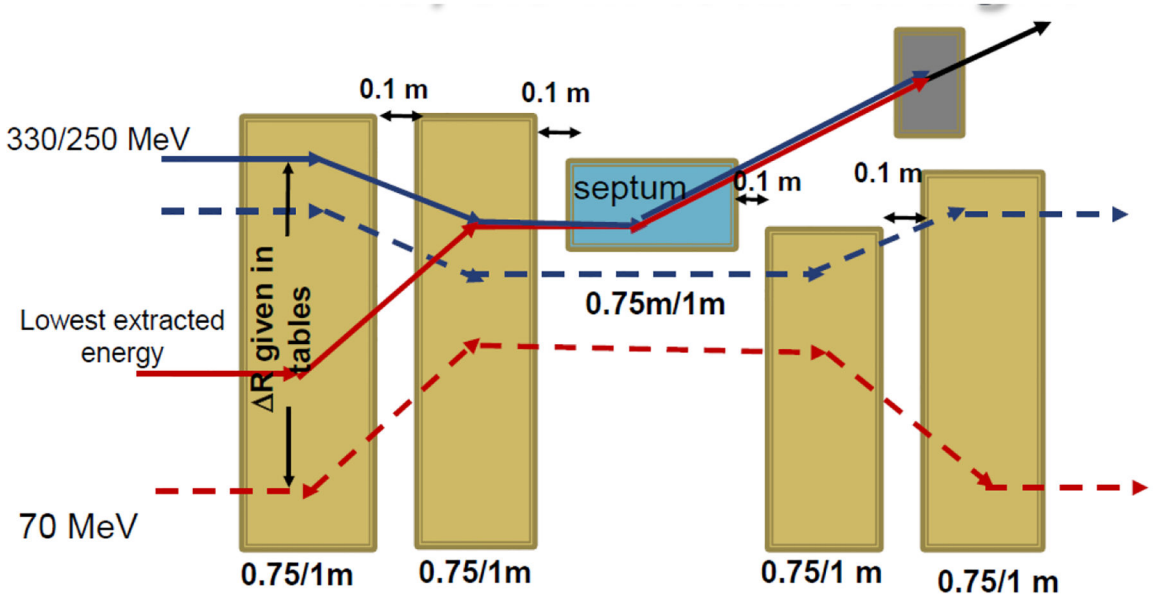

Figure 8.

Layout of the ramped, bipolar magnet extraction system that selects the orbit and energy for extraction through a septum. Inner, lower-energy orbits are returned to their respective closed orbits for continued acceleration. Reproduced from Ref. [50].

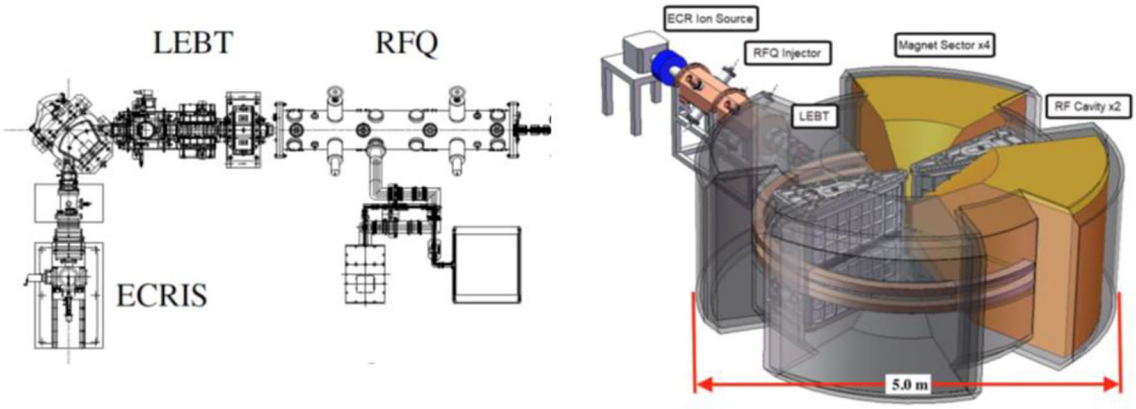

Figure 9.

HIMAC, Japan ion source, and RFQ (**left**), which serve as the concept for the upstream pre-acceleration system for the injector accelerator (**right**). A CAD model of the full conceptual design of the 20 MeV/u injector system (scalable to 70–100 MeV/nucleon) is shown on the right. From left to right, the ECR ion source, focusing solenoid, RFQ, beam focusing quadrupoles, and the cyclotron shown with a transparent outer shielding for clarity.

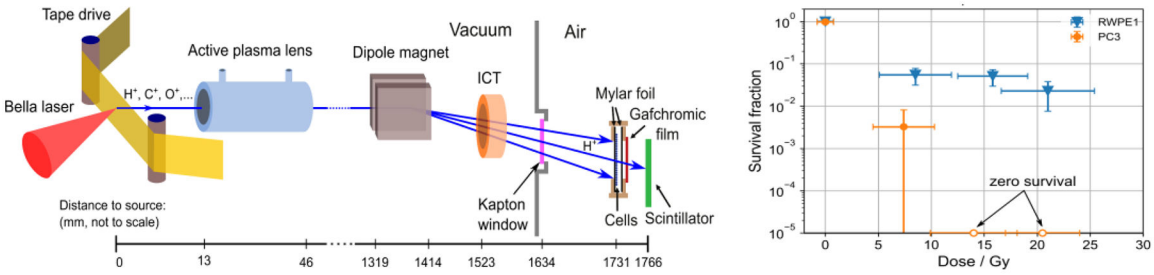

Figure 10.

Figure adapted from Ref. [88]. (**a**) Schematic depiction of the laser-driven proton beamline at the BELLA PW laser with tape-drive target, active plasma lens, dipole magnet, integrating current transformer (ICT), cell sample, radiochromic film, and scintillator. (**b**) Cell survival fraction of human prostate cancer cells (PC3) and normal human prostate cells (RWPE1) after irradiation with laser-driven protons. (J. Bin, et al. Sci Rep. 2022 Jan 27;12(1):1484. doi: 10.1038/s41598-022-05181-3, reproduced with permission under the terms of the Creative Commons Attribution License (CC BY), http://creativecommons.org/licenses/by/4.0/) (accessed on 9 September 2022).

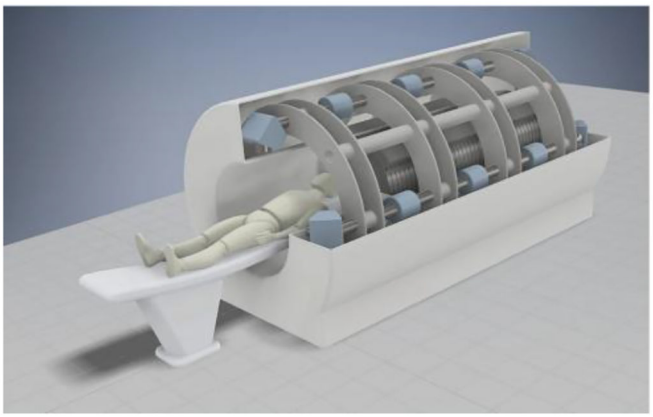

Parameter	Induction Linear Accelerator
Electron Energy (MeV)	16.0
Total Beam Current (A)	25.0
Pulse Width (s)	$1.5 \cdot 10^{-8}$
Pulse repetition Frequency (Hz)	10,000
Net Gradient (MeV/m)	5.0
Accelerator Length (m)	3.2
Inner Radius (cm)	10.0
Instantaneous Surface Dose Rate (Gy/s)	$6.6 \cdot 10^{5}$
Average Surface Rate (Gy/s)	98.9
Total Dose (Gy)	19.8
Time On (s)	0.2

Figure 11.

Concept FLASH-RT system using a linear induction accelerator (LIA) providing four or more lines of sight. LIA is on axis with the patient. Blue components are the magnetic focusing elements that direct the electron beam to the patient. The active accelerator is 3.2 m. With the returning drift section, the overall system length is 3.5 m less the patient couch [121]. (Sampayan, S.E.; et al., Sci. Rep. 2021, 11, 17104, https://doi.org/10.3389/fonc.2019.01563 (accessed on 9 September 2022), reproduced with permission under the terms of the Creative Commons Attribution License (CC BY), http://creativecommons.org/licenses/by/4.0/) (accessed on 9 September 2022).

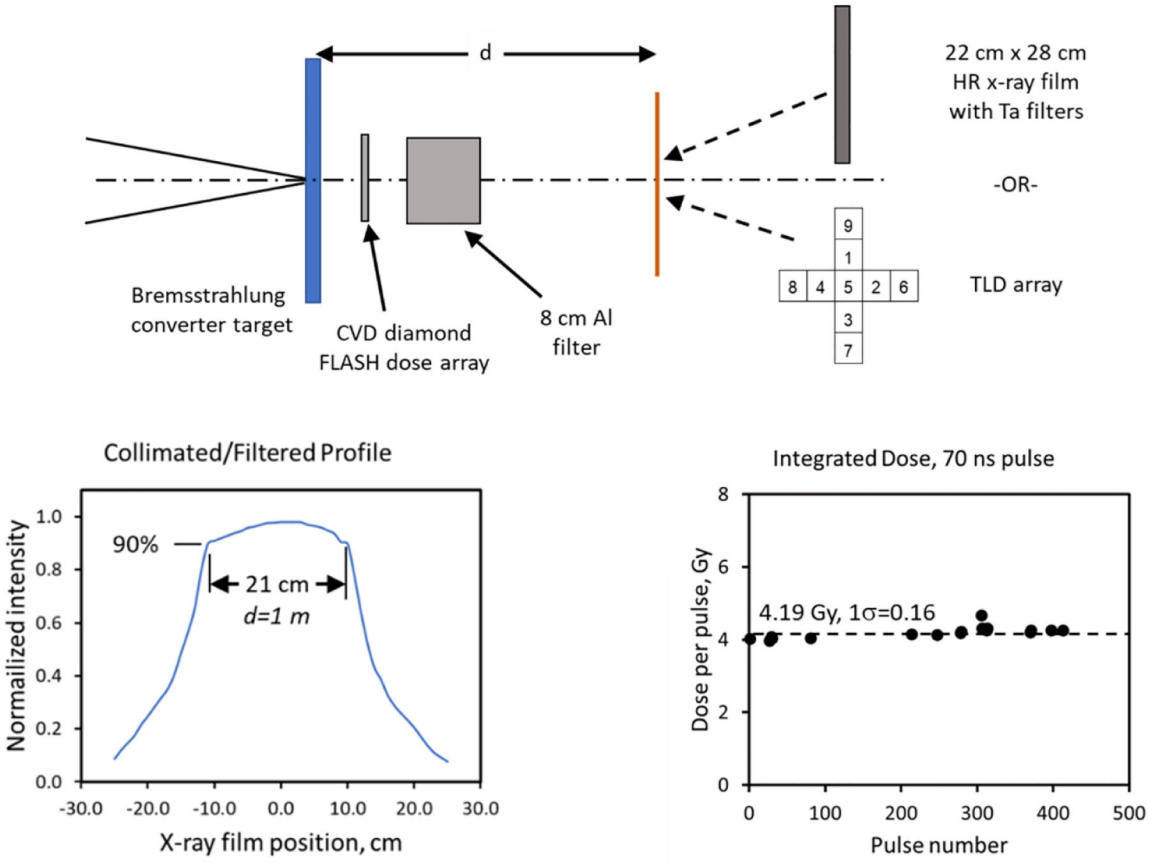

Figure 12.

Measurement geometry, bremsstrahlung field flatness, and pulse-to-pulse repeatability [121]. (Sampayan, S.E.; et al., Sci. Rep. 2021, 11, 17104, https://doi.org/10.3389/fonc.2019.01563 (accessed on 9 September 2022), reproduced with permission under the terms of the Creative Commons Attribution License (CC BY), http://creativecommons.org/licenses/by/4.0/) (accessed on 9 September 2022).

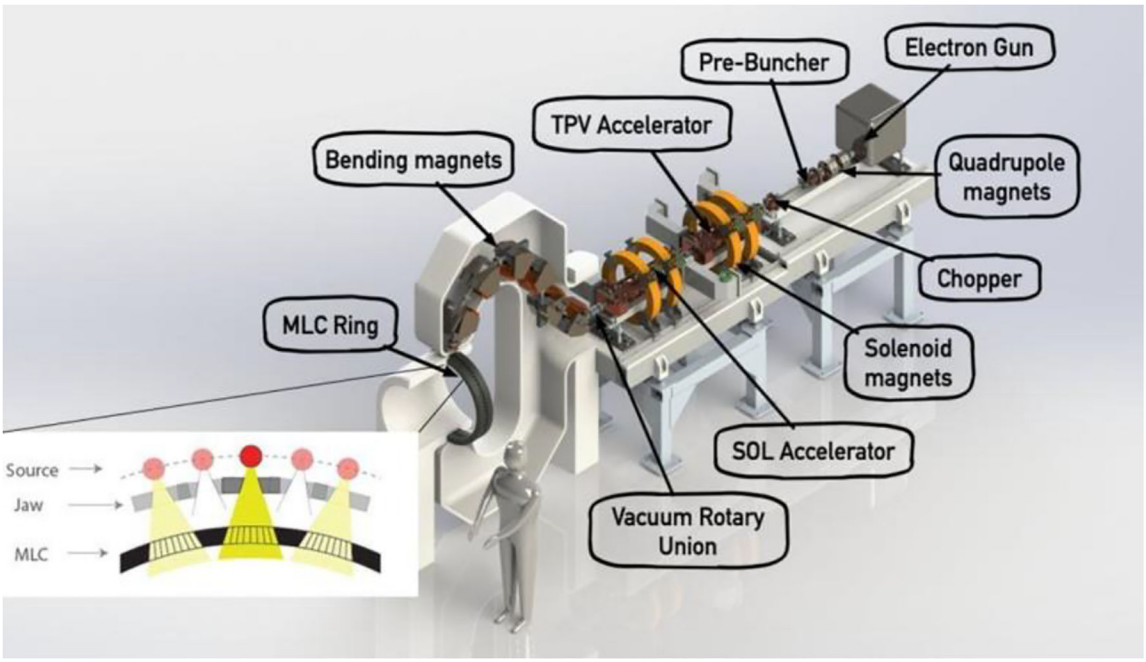

Figure 13.

Rendering of the ROAD FLASH-RT system. A segment of the decoupled MLC ring is shown in the figure inset with three MLC modules. The linac is triggered to produce the beam when the target is aligned with the MLC to produce a VMAT-like treatment.

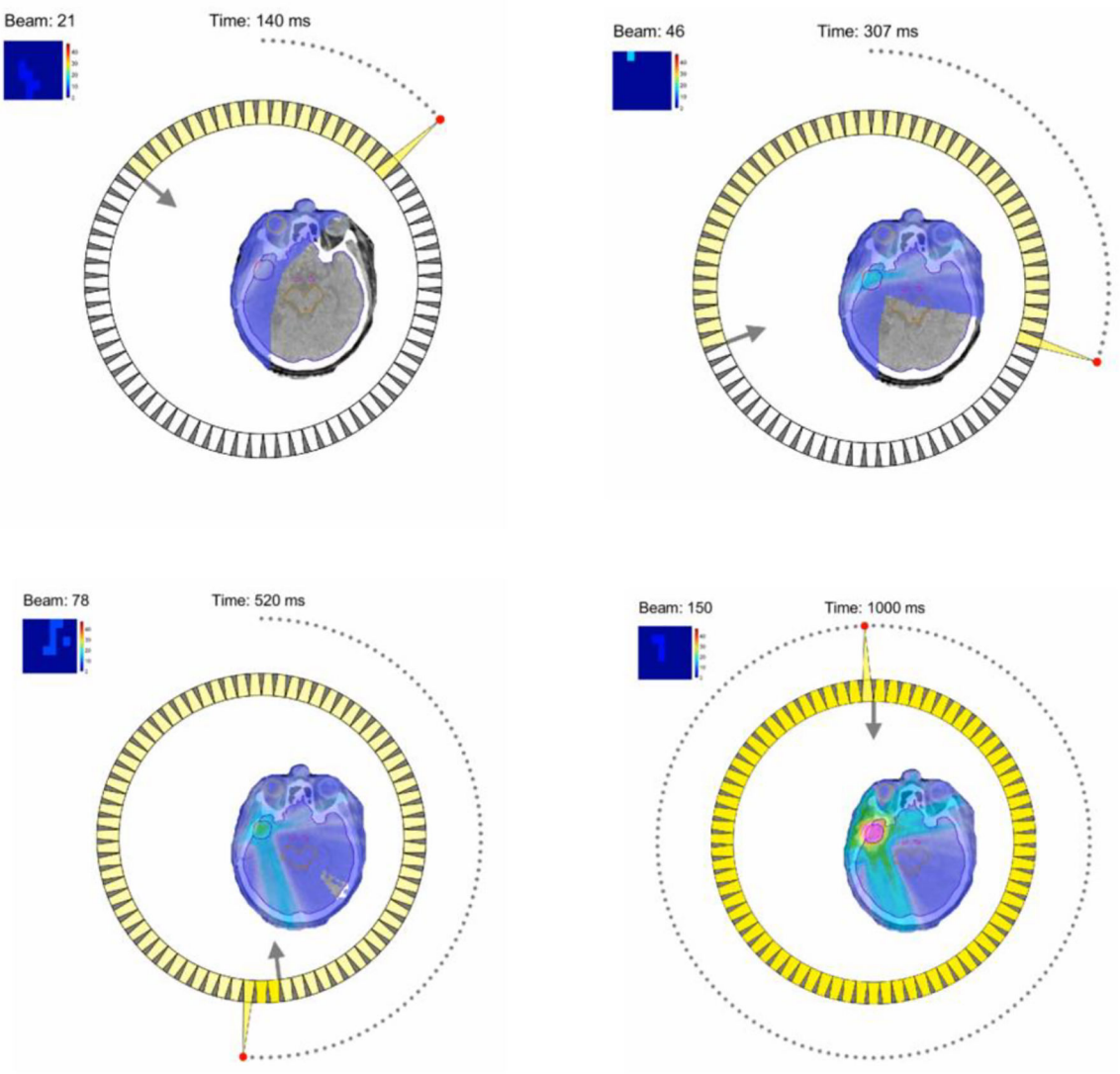

Figure 14.

FLASH-RT delivery using ROAD. The figure shows four beams with the corresponding pre-shaped MLC in the upper-left corner of respective beams. Cumulative radiation dose to a brain-tumor patient is shown in the center.

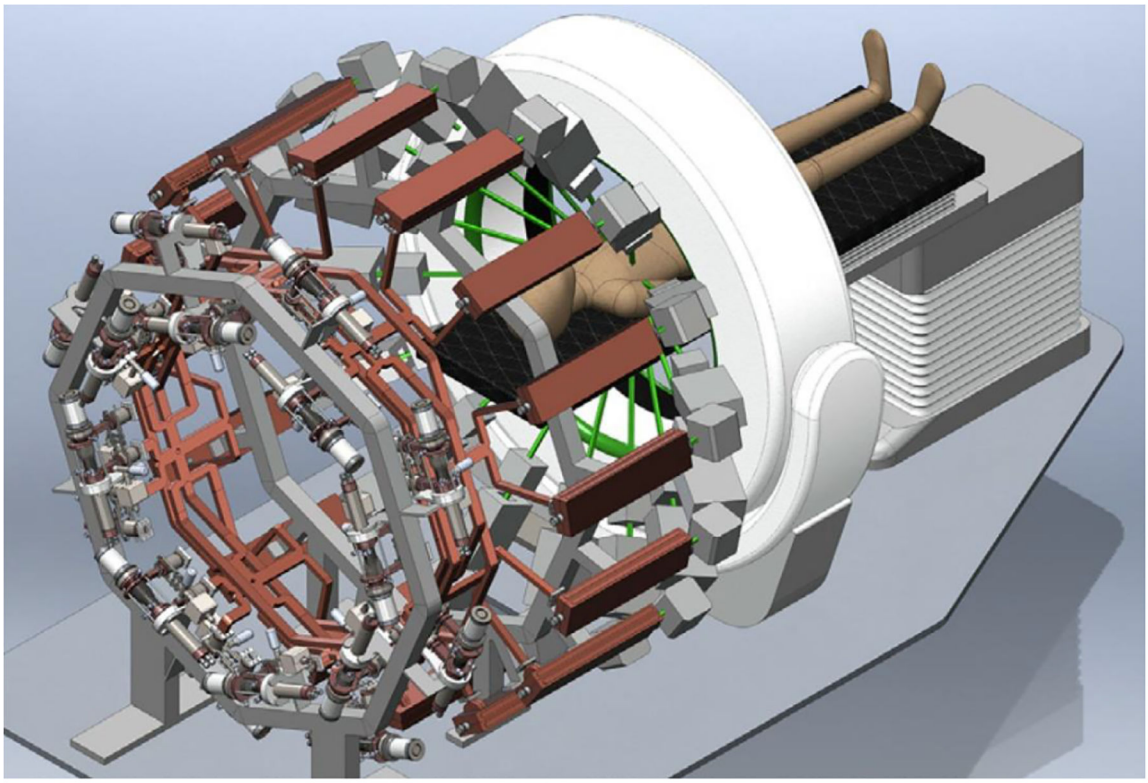

Figure 15.
Conceptual diagram of the PHASER architecture with 16 linacs arrayed around the patient for highly conformal FLASH photon therapy. Reproduced with permission from Ref. [141].

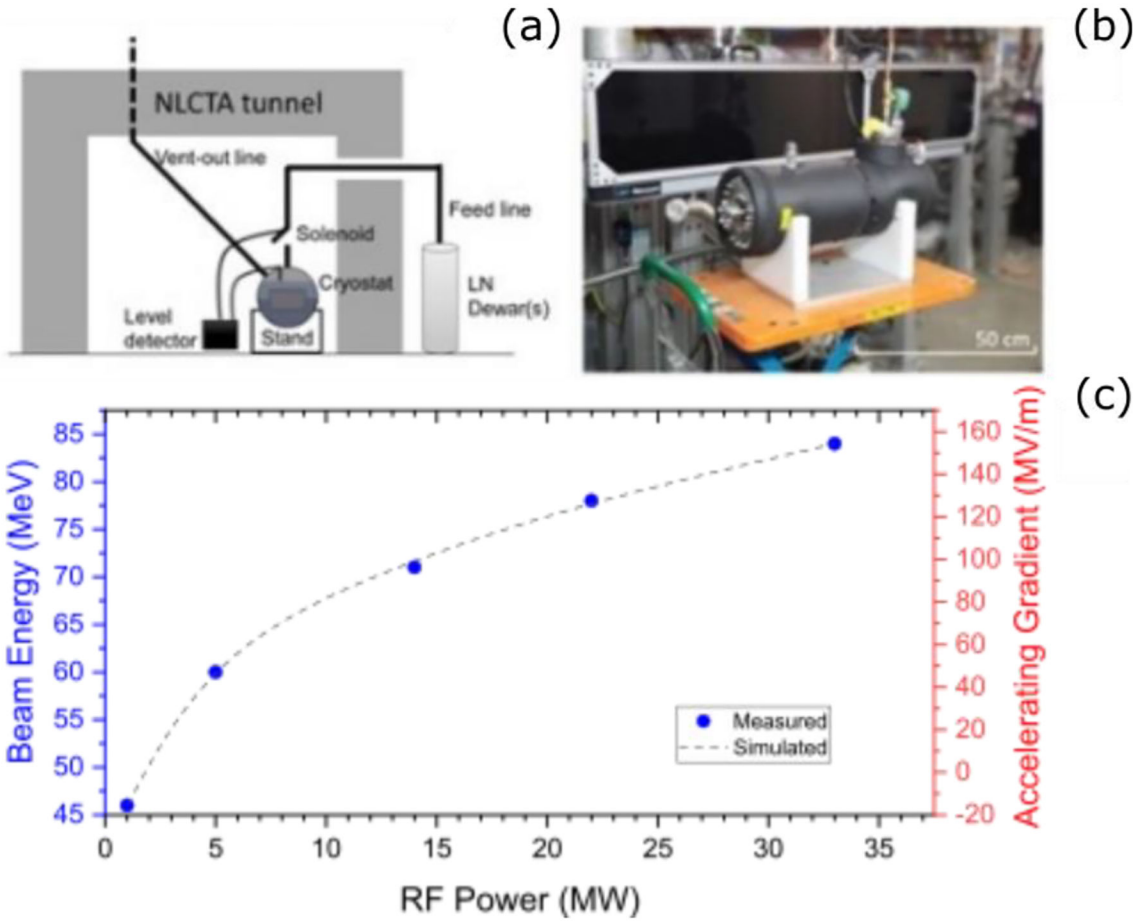

Figure 16.

(**a**) Schematic of cryogenic test setup at XTA using liquid nitrogen. (**b**) Photo of linac and cryostat assembly prior to installation at XTA. (**c**) Measurements of accelerating gradient as a function of RF power.

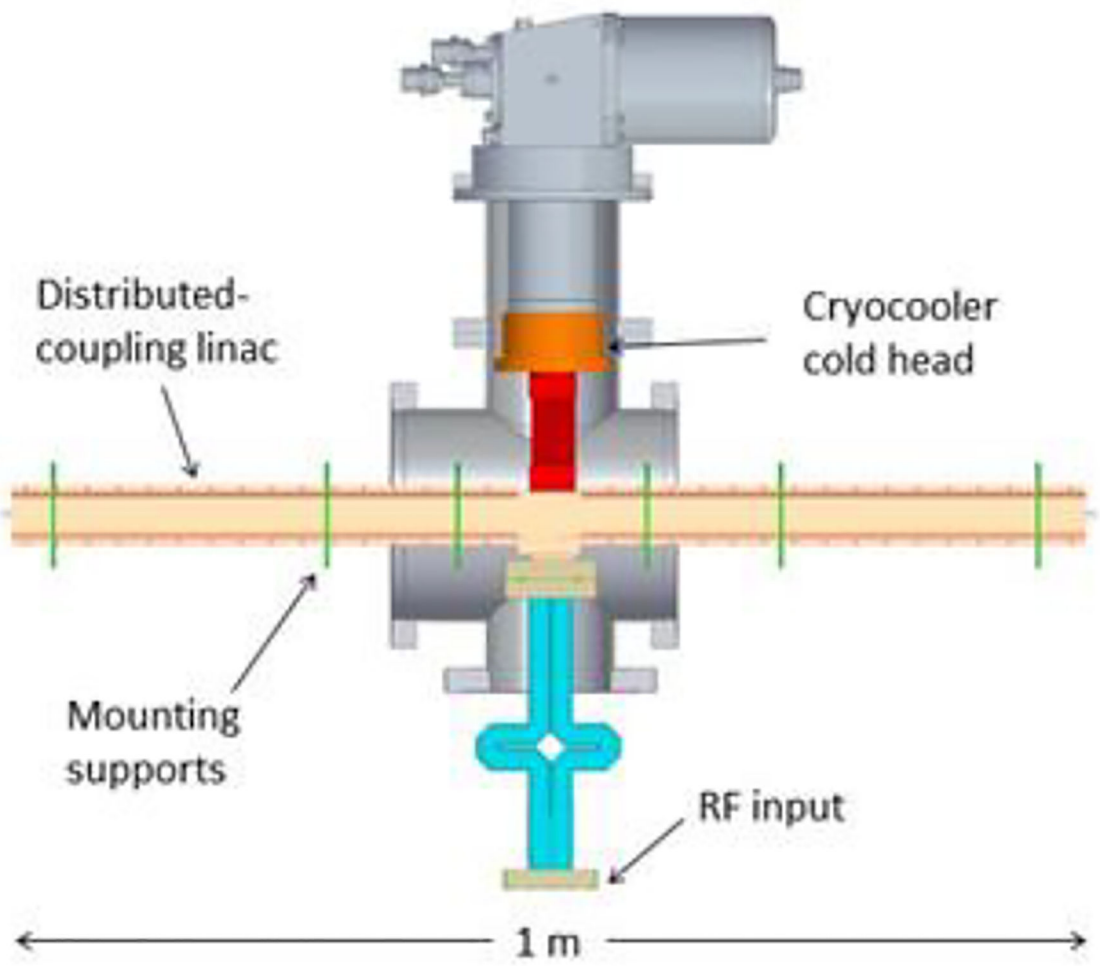

Figure 17.
Schematic of the cryogenic X-band linac for VHEE under development at SLAC.

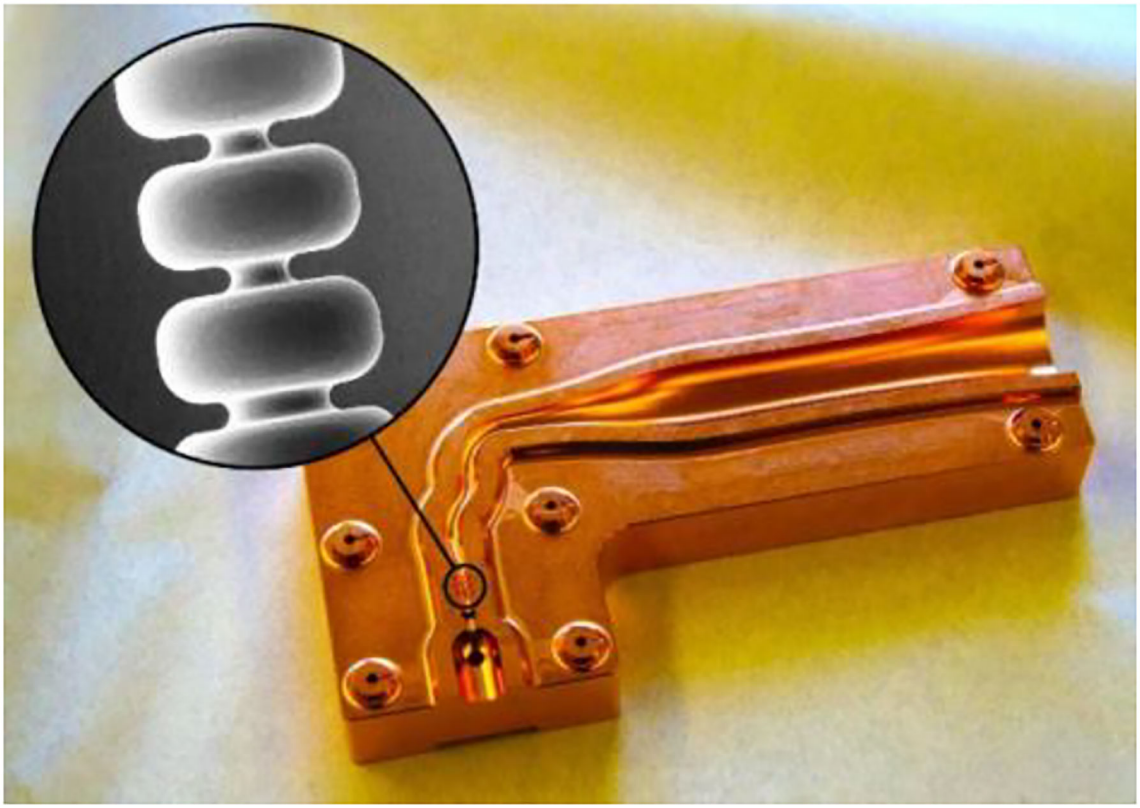

Figure 18.
SLAC mm-wave linac prototype for high-power testing.

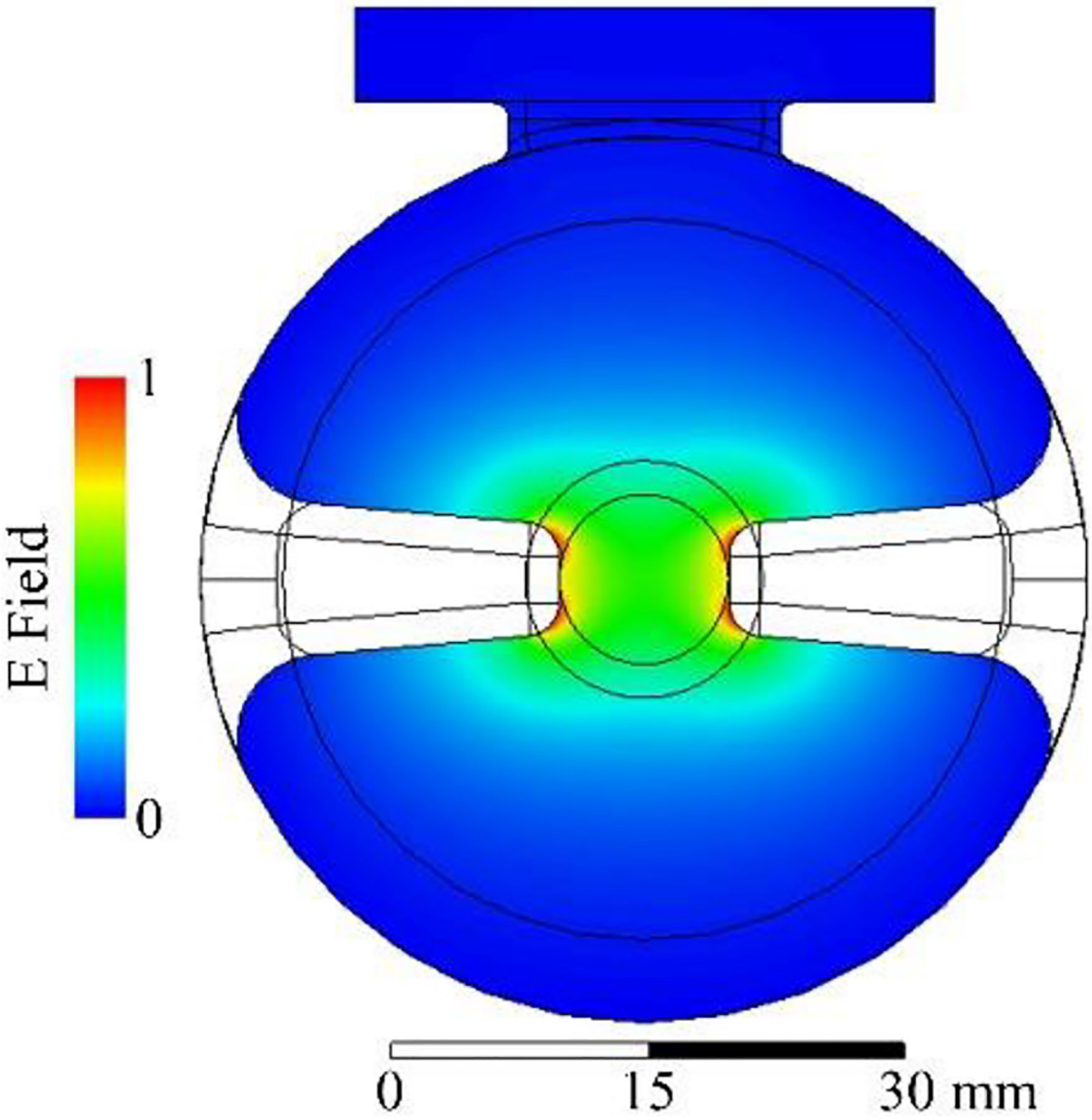

Figure 19.

Electric field profile of the TE11-like mode shown in a cross-section of the deflector cell, with beam axis oriented into the page. The opposing posts (profiles shown in white) produce an RF dipole. Power is coupled in through the port at the top of the model simulated in ANSYS-HFSS.

Table 1.

Preclinical electron FLASH properties relevant to a clinical application of FLASH.

Electron Beam	Min. for Observed FLASH	Optimal for FLASH
Average dose rate	30 Gy/s	100 Gy/s
Intrapulse dose rate	~10^5 Gy/s	≥10^6 Gy/s
Total dose	<10 Gy	≥10 Gy–tissue dependent
Delivery time for 10 Gy	<1 s	1 μs–10 ms

Table 2.

Dose delivery requirements for FLASH for protons and ions extrapolated from electron FLASH studies.

Dose Delivery Mode	Protons	Helium	Carbon
Conventional: 2.6 Gy/fraction	2×10^9 p/s	5×10^8 He/s	1.7×10^8 C/s
Delivery time: 100 s	0.4 nA	0.2 nA	0.2 nA
FLASH: ≥10 Gy/fraction	1×10^{13} p/s	2.5×10^{12} He/s	0.8×10^{12} C/s
Delivery Time: 100 ms	1.6 μA	0.8 μA	0.8 μA

Table 3.

Proton beam parameters for cell sample irradiations at the BELLA PW.

Beam Parameter	Value
Dose per pulse	1 Gy
Pulse length	30 ns
Pulse repetition rate	0.2 Hz
Instantaneous dose rate	3×10^7 Gy/s
Mean dose rate	0.2 Gy/s

Table 4.

Parameters of ROAD high-current electron linear accelerator for X-ray FLASH therapy.

System	ROAD	Conventional [18]
Energy [MeV]	18	6
Pulse length [μs]	167	4
Rep rate [Hz]	150	250
Duty cycle	2.5%	0.1%
Injected current [A]	1.3	0.5
Transmission	25%	25%
Peak current [A]	0.325	0.125
Average current [mA]	8.14	0.125
Dose rate factor [Gy/min/mA at 1 m]	2000	120
Dose rate, uncollimated, at 1 m [Gy/s]	**271**	**0.25**
Dose delivery efficiency	25%	25%
Dose rate, collimated, at 80 cm SAD [Gy/s]	**106.0**	**0.10**